# A Moist Linear Baroclinic Model: Coupled Dynamical–Convective Response to El Niño

Masahiro Watanabe[1*] and Fei–Fei Jin[2]

1. Division of Ocean and Atmospheric Science, Hokkaido University
   Nishi 5, Kita 10, Sapporo 060–0810, Japan
2. Department of Meteorology, School of Ocean and Earth Science and Technology
   University of Hawaii at Manoa, Honolulu, HI 96822-2219, USA

*Journal of Climate*

June 10, 2002, submitted

---

*Corresponding author:* Dr. M. Watanabe, E–mail: hiro@ees.hokudai.ac.jp

## ABSTRACT

A newly developed, linear baroclinic model (LBM) and its application to the tropical ENSO teleconnection is described. The model, based on primitive equations linearized about the observed, zonally varying basic state in northern winter, involves linear schemes for the cumulus convection, surface sensible and latent heat fluxes, referred to as the moist LBM. This enables us to solve a steady state response of the coupled dynamical–convective system to given SST anomaly, which is fairly different from the conventional dry LBM. Linear representation of the convection is acceptable for a realistic range of SST anomalies, reproducing well the Rossby wave train computed in the conventional LBM forced by a tropical heating.

We used the moist LBM to examine the formation mechanisms of an anomalous low–level anticyclone near Philippines which links El Niño with the Asian winter monsoon. Given that the conventional LBM simulates the Philippine Sea anticyclone as a Rossby response to the anomalous diabatic cooling associated with the weakened convection over the maritime continent, causes of the convective suppression is examined. Moist LBM experiments forced by observed El Niño SST anomalies indicate that a basin–wide warming of the Indian Ocean, in addition to SST anomalies in the Pacific, has a considerable impact in weakening the convection over the maritime continent through a modulation of the Walker circulation. Observational analysis supports this idea and further suggests that the lagged Indian Ocean response to El Niño contributes to determine when the Philippine Sea anticyclone is developed. The moist LBM identified a positive wind–evaporation feedback at work between the Philippine anticyclone and the western Pacific SST anomaly, which might also have some role.

# 1 Introduction

It is widely known that El Niño–Southern Oscillation (ENSO), the most prominent natural climate variability on interannual time scales, has a significant impact on the global atmosphere. One of the ENSO influence is apparent over the North Pacific where a wavy geopotential height anomaly pattern that resembles the Pacific/North American (PNA) teleconnection dominates during El Niño and La Niña years (Horel and Wallace 1981). ENSO is found to modulate the monsoon activity over Asian regions as well (Webster et al. 1998, and references herein).

So far, anomalous atmospheric circulation associated with El Niño has often been discussed in terms of forced steady responses to the diabatic heating anomaly induced by the enhanced convections over the central–eastern Pacific. Hoskins and Karoly (1981) first demonstrated that the PNA–like height anomaly is interpreted as a Rossby wave train excited by the tropical heating although several papers later pointed out other factors in midlatitudes such as a feedback from transient disturbances (Held et al. 1989, Hoerling and Ting 1994) and zonal inhomogeniety in the time mean flow (Branstator 1985) appear to have roles in forming the PNA pattern as important as the heating in the tropics. On the other hand, Nigam (1994) showed that the El Niño heating over the tropical regions regulates low–level westerly flow hence affects the intensity of the Asian monsoon in the subsequent season.

Many of studies cited above have utilized a linear baroclinic model (hereafter referred to as LBM) to obtain the steady atmospheric response to a prescribed heating. Those studies present that the LBM is an useful tool to diagnose how the atmosphere dynamically reacts convective heating which is fixed both in space and in time. However, cumulus convections generating the anomalous heat source are in reality coupled with the circulation and they can be interacting with the large–scale dynamics. When convection anomaly excites an anomalous atmospheric circulation that has much larger scale than the heating, an additional convection anomaly in response to the circulation response may occur in a remote region and in turn force the atmosphere. Such a process is especially likely to happen in the tropics, therefore a question which we raise here is; does the steady atmospheric response *under the coupling*

*with interacting diabatic processes* differ from the response pattern determined by uncoupled, prescribed heating? Furthermore, if it does, how? Motivated by this question, we describe in this study an attempt to obtain forced steady responses of the coupled dynamical–convective system using the LBM.

Free modes in the dynamical–convective system have been extensively investigated in a framework of the conditional instability of the second kind (CISK). In particular, many efforts have been made to extract unstable modes which arise from a feedback between convective heating and the low–level convergence associated with tropical waves, called wave–CISK (e.g. Yamasaki 1969; Hayashi 1970; Lindzen 1974; Stevens and Lindzen 1978). While these modes are relatively sensitive to the choice of cumulus parameterization and even stabilized with some schemes (Stark 1976; Crum and Stevens 1983; Brown and Bretherton 1995), they are proposed as a possible mechanism for the tropical intraseasonal oscillations (Lau and Peng 1987; Chang and Lim 1988; Sui and Lau 1989). As mentioned, however, these studies mainly focused on to obtain modal solutions with relatively simplified (e.g. two dimensional model, equatorial $\beta$ plane, and idealized basic states) conditions. On the other hand, the present study examines forced solutions in more realistic, three dimensional states. In the first half of this paper, we detail the numerical model and compare results of the LBM including moist diabatic processes, referred to as the moist LBM, with those of the conventional LBM. Then an application of the moist LBM computations is presented in the latter half, which is aimed to further understand the teleconnection associated with ENSO as explained below.

During the mature phase of El Niño, sea level pressure shows large positive anomalies over the western subtropical Pacific, which are lasting into the spring (Harrison and Larkin 1996). Wang et al. (2000, hereafter denoted as WWF) also exhibited that an anomalous anticyclonic circulation near Philippines that is associated with the positive sea level pressure anomalies and is confined to the lower troposphere rapidly develops during autumn prior to the El Niño mature. This anticyclonic anomaly counteracts the northerly wind of the Asian winter monsoon and supplies more water vapor from the south, hence contributes to wet and

mild conditions over East Asia. WWF further carried out atmospheric general circulation model (AGCM) experiments which suggest that the Philippine Sea anticyclone is forced by suppressed convective heating over the maritime continent while maintained through the positive wind–evaporation feedback with in-situ sea surface cooling. The moist LBM which we have developed is applied to verify the WWF's hypothesis by solving coupled dynamical–convective responses to sea surface temperature (SST) anomalies associated with El Niño. We found that some results are fairly consistent with WWF, for example, the Philippine Sea anticyclone was excited by the suppressed convection over the maritime continent. However, it was also shown that the weakening of convections results from a modest warming in the Indian Ocean SST, in addition to the strong El Niño SST anomaly in the central–eastern Pacific. A delayed warming of the Indian Ocean SST appears to be responsible for the rapid development of the anomalous anticyclone near Philippines.

This paper is organized as follows. In section 2, LBM and moist processes involved are described. A forced response in the moist LBM is compared with the conventional LBM response and observations in section 3, in order to validate the model formulation. Section 4 gives a physical insight into the mechanism of suppressed convections and associated anticyclonic circulation over the western tropical Pacific based on results of the moist LBM experiments, followed by some observational data analyses presented in section 5. The finding obtained in this study is summarized and further discussed in section 6, with several remarks noticed in the last section.

# 2 Model description

### *a. Linear baroclinic model*

The LBM used in this study is based on primitive equations exactly linearized about a basic state (see Watanabe and Kimoto 2000, 2001 for mathematical expressions). The model variables which consist of vorticity ($\zeta$), divergence ($D$), temperature ($T$) and logarithm of

surface pressure ($\pi$) are horizontally represented by spherical harmonics having the resolution of T21 while vertically discretized using a finite difference on to 20 $\sigma$ levels, in which five layers reside below $\sigma = 0.8$. In most computations presented in this article the basic state is adopted from the zonally varying, winter (December–February) climatology of the NCEP reanalysis. The model also includes three dissipation terms: a biharmonic horizontal diffusion with the damping time scale of 1dy for the smallest wave, very weak vertical diffusion (damping time scale of 1000dy) to remove a vertical noise arising from finite difference, and the Newtonian damping and Rayleigh friction as represented by a linear drag which has a time scale of 1dy applied only to the lower boundary layers ($\sigma \geq 0.9$) and the uppermost two levels ($\sigma \leq 0.03$).

### *b. Basic concept of the moist LBM*

An extension of the linear model which includes an interacting convection is briefly explained here, followed by description of schemes for the diabatic processes in section 2c.

A steady linear response is symbolically written as

$$\mathsf{L}\mathsf{X} = \mathsf{F} \quad , \tag{1}$$

where $\mathsf{X}$ is a vector containing perturbations $(\ )'$ for prognostic variables, i.e., $\mathsf{X} \equiv \mathsf{X}(\zeta', D', T', \pi')$,

while $\mathsf{F}$ and $\mathsf{L}$ denote a prescribed forcing and linear dynamical operator, respectively. When we consider the forcing solely due to anomalous cumulus convection, Eq. (1) can be solved with a given diabatic heating as $\mathsf{F}$, referred to as the dry LBM. When the anomalous convective heating is internally generated in response to SST anomaly, $\mathsf{F}$ will be a function of both $\mathsf{X}$ and an SST anomaly $T_s'$ in addition to a basic state $\overline{\mathsf{X}}$. Then it can be decomposed into two components, $\mathsf{F}_i(\overline{\mathsf{X}})\mathsf{X}$ and $\mathsf{F}_e(\overline{\mathsf{X}}, T_s')$ ('$i$' and '$e$' stand for internal and external, respectively), so that Eq. (1) is rewritten as

$$(\mathsf{L} - \mathsf{F}_i)\mathsf{X} = \mathsf{F}_e \quad . \tag{2}$$

Note that $\mathsf{X}$ in Eq. (2) now includes perturbation in the specific humidity $q'$. The heat source and moisture sink induced by anomalous convection are represented by $\mathsf{F}_i\mathsf{X}$. In the

linear model expressed by Eq. (2), which is the moist LBM, a forcing $\mathsf{F}_e$ is composed by terms in linearized surface bulk fluxes that depend on $T_s'$ and the basic state but not on the perturbation $\mathsf{X}$, as further delineated later. Actual implementation for $\mathsf{F}_i$ and $\mathsf{F}_e$ is described in the next section.

Since the rank of $\mathsf{L}$ and $\mathsf{L}-\mathsf{F}_i$ exceeds 30000 with the resolution employed, it is hard to solve Eqs. (1) and (2) with the matrix inversion technique. Instead, we integrate the models in time to obtain the state state response. While the time integration fails to capture steady response when unstable modes such as baroclinic waves dominate, the boundary layer damping of $(1\mathrm{dy})^{-1}$ is enough in neutralizing those modes (cf. Hall and Sardeshmukh 1998), that ensures the steady state response can be obtained in this method. In fact, we have confirmed that steady responses by the time integration are qualitatively similar to those obtained by the matrix inversion with much lower resolution of T21 and vertical 11 levels. Both for the dry and moist linear models, the time integration is continued up to 30 days, while the responses at day 15 are only shown in the subsequent section because the tropical response approaches steady state approximately after day 10 or 15.

### *c. Cumulus convection and surface fluxes*

For the state vector of the moist LBM, $\mathsf{X} \equiv \mathsf{X}(\zeta', D', T', \pi', q')$, forcing $\mathsf{F}$ contains the following components.

$$\mathsf{F} \equiv \mathsf{F}(0, 0, Q_c' + Q_h', 0, Q_q' + Q_e') \quad ,$$

where $Q_c'$ and $-Q_q'$ denote the convective heat source and moisture sink while $Q_h'$ and $Q_e'$ are the surface sensible and latent fluxes, respectively.

The cumulus convection is represented as

$$Q_c' = \frac{e_c}{\tau_c}(T_c' - T' - \Delta T_c') \quad , \tag{3}$$

$$Q_q' = \frac{e_c}{\tau_c}(q_c' - q') \quad . \tag{4}$$

They are based on a relaxed convective adjustment proposed by Betts (1986) and Betts and Miller (1986), further following a linearization by Neelin and Yu (1994). When cumulus convection occurs, temperature and specific humidity perturbations are restored to reference profiles $T'_c$ and $q'_c$ with an adjustment time $\tau_c$. The time scale of the adjustment basically follows the life time of convective clouds, here set at 2hr as in Betts (1986). $\Delta T'_c$ denotes a correction term which ensures the constraint between heat release and moisture consumption while $e_c$ indicates the so–called convective efficiency introduced in this study.

The convective adjustment is applied between the top of PBL, $\sigma_b$, and the cloud top $\sigma_t$. The value of $\sigma_b$ is fixed in space at 0.98 while $\sigma_t$ is defined by the level where cloud parcel raising from the boundary layer loses buoyancy.

Reference profiles $T'_c$ and $q'_c$ may be expressed in terms of the moist static energy at PBL, $h'_b = c_p T'_b + L q'_b$ ($T'_b$ and $q'_b$ are values in the PBL), as

$$c_p T'_c = A h'_b \quad , \tag{5}$$

$$L q'_c = B h'_b \quad . \tag{6}$$

Reference vertical profiles for $T'_c$ and $q'_c$, denoted as $A$ and $B$, are fixed in time and obtained in a slightly different manner from Neelin and Yu (1994). In the original scheme the reference profiles are determined by an iterative computation starting from the observed structure as initial $T_c$ and $q_c$ (Betts 1986). The final profile does not necessarily follow the moist adiabat, but close to it, as justified by Manabe and Strickler (1964). Therefore we simply assume the cloud parcel raising with preserving the moist adiabatic character from the PBL, namely,

$$c_p T'_c + \phi'_c + L q'_s(\overline{T}, T'_c) = c_p T'_b + \phi'_b + L q'_b \quad , \tag{7}$$

where $q'_s$ is a perturbation of saturated specific humidity defined as

$$L q'_s = \gamma c_p T'_c \quad , \tag{8}$$

$$\gamma = \frac{L}{c_p} \frac{dq_s}{dT} \mid_{T=\overline{T}} \quad . \tag{9}$$

By applying the hydrostatic equation for $\phi'_c$ and $\phi'_b$, Eq. (7) is analytically solved for $A$ (cf. Yu and Neelin 1994),

$$A = \frac{1}{(1+\gamma)} \exp[-\kappa \int_{\sigma}^{\sigma_b} \frac{1}{(1+\gamma)\sigma} d\sigma] \quad . \tag{10}$$

The moist adiabat assumption also leads to a saturated condition

$$\overline{q}_c + q'_c = q_s(\overline{T}) + \frac{c_p}{L}\gamma T'_c \quad , \tag{11}$$

which then gives the profile for $B$ simply as

$$B = \gamma A \quad . \tag{12}$$

Examples of $A$ and $B$ are displayed in Fig. 1, which shows the vertical section along 180°E computed with the winter basic state. As expected from an observational estimate of the heat source and moisture sink, $A$ and $B$ have the maximum in the upper and lower troposphere, respectively. It should be noted, however, that vertical structure of $Q'_c$ and $Q'_q$ internally calculated in the model may not necessarily resemble $A$ and $B$ since the heat source and moisture sink depend on the environmental values of temperature and humidity as well.

While $Q'_c$ and $Q'_q$ are independently determined both by means of $h'_b$, they must satisfy an energy constraint of the heating balanced by the moisture sink at each column:

$$c_p \int_{\sigma_t}^{\sigma_b} Q'_c d\sigma + L \int_{\sigma_t}^{\sigma_b} Q'_q d\sigma = 0 \quad . \tag{13}$$

In principle, the energy constraint can be achieved by modifying $T'_c$ and $q'_c$ such as to satisfy Eq. (7) with $\Delta T'_c = 0$ through an iterative adjustment (Betts and Miller 1986). Here, however, we avoid such an iteration and instead give the correction term $\Delta T'_c$ led by substituting Eqs. (2)–(6) into Eq. (7),

$$\Delta T'_c = c_p^{-1}[(< A > + < B >)h'_b - c_p < T' > -L < q' >] \quad , \tag{14}$$

where $<\quad>$ means a vertical average between the cloud base and top.

In nature, the deep cumulus convection only occurs where the environment provides sufficient buoyancy to the cloud parcel, which is measured either by CAPE or the cloud work function. In the original Betts (1986) scheme, such a constraint has not been explicitly included although $\sigma_t$ reflects the basic state CAPE. Therefore, the convective efficiency $e_c$ which represents the constraint from the basic state CAPE is multiplied to Eqs. (3)–(4) according to the definition

$$e_c = \min\left(\frac{\overline{M}}{M_c}, 1-\epsilon\right) \quad , \tag{15}$$

where $\overline{M}$ indicates a basic state CAPE while $M_c$ is a critical value of CAPE set at 3000 J Kg$^{-1}$. A limitation parameter $\epsilon$, to which a tiny value of 0.1 is given, is to mimic that not all the available moist energy is converted to the cumulus heating. The basic state CAPE and $e_c$ are shown in Fig. 2. The CAPE has a broad maximum in the entire tropics except for the Pacific and Atlantic cold tongues (Fig. 2a). The maximum resides in the Southern Hemisphere because we chose the northern winter as the basic state. The convective efficiency follows the distribution of CAPE, confining cumulus convections to the tropics except for the western North Pacific and Atlantic where baroclinically unstable flow can result in a weak convective rainfall (Fig. 2b). It should be noted that $e_c$ plays a minor role in determining a forced dynamical–convective response therefore results are similar to even with $e_c = 1$ everywhere (not shown).

The source of convective anomalies is the sensible and latent heat supplied at surface. They are provided by the respective linearized form of the Bulk formula:

$$Q'_h = \frac{g}{\overline{P_s}\Delta\sigma_b}\rho C_h[\overline{W}(T'_s - T') + W'(\overline{T_s} - \overline{T})] \quad , \tag{16}$$

$$\begin{aligned} Q'_e &= \overline{\beta_e}\frac{g}{\overline{P_s}\Delta\sigma_b}\rho C_e[\overline{W}\{c_p L^{-1}\gamma(\overline{T_s})T'_s - q'\} + W'\{q_s(\overline{T_s}) - \overline{q}\}] \\ &\quad + \beta'_e\frac{g}{\overline{P_s}\Delta\sigma_b}\rho C_e[\overline{W}\{q_s(\overline{T_s}) - \overline{q}\}] \quad , \end{aligned} \tag{17}$$

where the bulk coefficients $C_h$ and $C_e$ are calculated with basic state quantities, following Louis (1979). We assume the PBL thin enough, so that $Q'_h$ and $Q'_e$ are uniformly given in the PBL. The wind speed is indicated by $\overline{W}$ and $W'$ in Eqs. (16)–(17), with the perturbation expressed as

$$W' = \frac{1}{\overline{W}}(\overline{u}u' + \overline{v}v') \quad , \tag{18}$$

where we set the minimum of $\mid \overline{W} \mid$ at 2.5 m s$^{-1}$ to avoid singularity near the border between the surface easterly and westerly in the basic state. $\overline{\beta_e}$ represents an evaporation efficiency, which is always 1 over oceans while takes various values over lands depending upon the soil moisture $\overline{W_g}$. In this study, $\overline{\beta_e}$ is fixed at 0 over lands for simplicity. In addition, perturbation in the evaporation efficiency $\beta'_e$ which is a function of $W'_g$ and has nonzero value only over land is also set at 0 since the model yet includes a prognostic equation for $W'_g$. As a results, the current scheme lacks an atmosphere–land coupling in terms of latent heat exchange, which is further discussed in section 6. Nevertheless, this caveat is not likely to affect results presented in the present paper since most of convective heating focused on concentrates over oceans.

In summarize, the convection and surface flux schemes are driven by $T'_s$ given to Eqs. (16)–(17). The symbolic form of the external forcing $\mathsf{F}_e$ therefore consists of first terms in these equations while all the other terms in Eqs. (3)–(4) and (16)–(17) is internally computed in conjunction with the dynamical response, namely, indicated ad $\mathsf{F}_i$ in Eq. (2). Note that terms involving $W'$ in Eqs. (16)–(17) represents the heat flux components induced by the anomalous wind, referred to as the wind–evaporation feedback although it contains the sensible heating as well. If the surface wind anomaly forced by a positive SST anomaly counteracts the mean wind, resultant $Q'_e$ produced by the negative $W'$ helps maintain the SST anomaly. Such a feedback is known to play an important role in the mean climate (e.g. Xie and Philander 1994) and we also examine the effect of the wind–evaporation feedback in a forced steady response in section 4c.

# 3 Model validation

In order to verify that the moist LBM works properly, we first focus on the in–situ diabatic heating and extratropical circulation anomalies associated with ENSO.

In Fig. 3, observed composite anomalies (differences between El Niños and La Niñas) in boreal winter are shown for three quantities: SST, outgoing longwave radiation (OLR) and geopotential height at 500 hPa. Here SST is derived from the UK Meteorological Office (Parker et al. 1995) while OLR is obtained from NOAA satellites available from June 1974 to November 1998 (Liebmann and Smith 1996). Products of the NCEP/NCAR reanalysis (Kalnay et al. 1996) are used for 500 hPa height and other atmospheric fields which will be shown later. Composites were made in reference to the Niño 3 SST index for 1949–1999 and winter anomalies during the same period except for OLR which has the data only available after 1979.

These anomalies associated with ENSO are briefly documented although many aspects of them would be already familiar. The strongest SST warming of maximum about 4 K is found in the central–eastern equatorial Pacific, accompanying weak negative anomalies in the western Pacific and midlatitude in both hemispheres (Fig. 3a). A modest warming also occurs in most parts of the Indian Ocean, which is known to have a delay in its development relative to the El Niño cycle (e.g. Tourre and White 1995; Lanzante 1996). In association with the SST signal in region I marked in Fig. 3a, there are extremely enhanced convections as inferred from negative OLR anomalies (Fig. 3b). They are surrounded by a horse–shoe pattern of positive OLR anomalies to their west, north and south. In the equatorial strip outside of the Pacific, convections are all suppressed except for the western Indian Ocean. The height composite is predominated by quadrapole anomalies over the North Pacific, some of which resemble the PNA teleconnection. Simultaneously, the entire tropics is covered by weak, but quite significant positive height anomalies reflecting the tropical–wide warming.

As detailed in section 2, the moist LBM forced by a prescribed SST anomaly calculates diabatic heating anomaly such as to balance with a steady circulation response. Figure 4 presents the depth–averaged heating response (denoted as $< Q_c' >$ following Eq. (14)) in

the experiment M1, in which SST anomalies in region I are given, for individual grid over the equatorial Pacific of 170°E–90°W and 10°S–10°N together with the corresponding observed OLR anomalies. Note that the $< Q_c' >$ and OLR are plotted against the common SST anomaly at each grid point. The scatter diagram for observed OLR (Fig. 4a) reveals that El Niño and La Niña are not symmetric in terms of the anomalous heating and cooling generated by them, namely, the former stronger than the latter. This asymmetry is likely to result from nonlinearity in the Clausius–Clapeyron equation which leads to larger sensitivity of $q_s'$ to positive SST anomaly. The heating anomaly diagnosed in the moist model is, however, nearly linear with respect to the phase of SST anomaly (Fig. 4b), which is trivial from the linear form of moist schemes. This indicates that the moist LBM may underestimate steady response to large positive SST anomaly such as 1997/98 El Niño. However, this model caveat is less clear for statistical ensemble anomalies as represented by El Niño–La Niña composites (orange dots in Fig. 4), suggesting that the linear representation of diabatic processes are acceptable for SST anomalies not extremely positive.

Another verification of the moist LBM is to compare the spatial structure of the heating and circulation responses with the observed heating and circulation response to it computed by the dry LBM (Fig. 5). For comparison with M1, the dry LBM was forced by the heating corresponding to the negative OLR anomaly over the equatorial Pacific (cf. Fig. 3b) with the vertical profile defined by an empirical function proposed by Reed and Recker (1971). The anomalous heating, $< Q_c' >$, calculated in this way shows the maximum of about 3 K day$^{-1}$ (Fig. 5a), which excites a Rossby wave train emanating toward North America as seen in the 500 hPa height response (Fig. 5b). In the moist LBM, $< Q_c' >$ over the equatorial Pacific is much stronger and zonally elongated compared to the empirically derived $< Q_c' >$ (Fig. 5c). Besides, anomalous cooling occurs over the regions away from SST anomalies, which must have been induced by the anomalous circulation. It is comprehensible that the cooling anomalies are caused by enhanced subsidence of the Hadley and Walker circulations driven by the strong upward motion over the equatorial Pacific. The diabatic cooling anomaly over the subtropical

Pacific and Amazon resembles the observed OLR anomalies whereas the observed convection anomalies are not well captured over the Indian Ocean and western Pacific, which will be discussed in the next section. It is also interesting to note that the PNA–like height response is nevertheless similar to that in the dry LBM, suggesting it being insensitive to the additional cooling appeared in the most LBM although the moist model is capable of better reproducing the wave train over the South Pacific and the low pressure anomaly over the North Pacific (Fig. 5d). Overall feature of the height response in the moist LBM is at least comparable to the dry LBM, indicating the relevance of the model formulation. Note that, however, the extratropical height responses in both models are weaker than observed composite (Fig. 3c) and reveal more wave–like structure. These deficiencies mostly arise from the absence of the transient eddy feedback (e.g. Held et al. 1989). In fact, the anomalous eddy momentum forcing associated with Fig. 3, computed using daily NCEP reanalysis data, is found to amplify and modify the height response toward observed anomalies over the North Pacific (not shown).

# 4 Model application: Why western Pacific convections are suppressed during ENSO?

In this section we further present steady responses diagnosed in the moist LBM which focused on the anomalous Philippine Sea anticyclone and convective activity over the western Pacific as described in the introduction.

## *a. Dry LBM experiments*

We first reexamine the WWF's argument that the Philippine Sea anticyclone is excited by the anomalous cooling associated with suppressed convections over the maritime continent but not by the heating over the central Pacific. The question if it is true can be qualified by means of the dry LBM with and without the cooling anomaly as prescribed forcing. Figure 6a shows the observed composite for the 850 hPa stream function (denoted as $\psi_{850}$) anomalies associated with ENSO superimposed on the OLR anomalies which have been shown in Fig. 3b. The

Philippine Sea anticyclone is found to dominate in the northwest of suppressed convections which also accompany a weak anticyclonic circulation anomaly over the Southern Hemisphere. The spatial phase of these anomalous anticyclones to the weakened convections does match the classical Gill–pattern (Gill 1980) except for the sign reversed. Indeed, the dry LBM forced only by the El Niño heating in the central Pacific lacks the anticyclonic responses over the western Pacific (Fig. 6b) whereas they are realistically reproduced when the anomalous cooling was incorporated (Fig. 6c). Note that the heating and cooling that force the dry LBM referred to the observed OLR anomaly pattern and adopted an empirical vertical function as in Fig. 4a. The $\psi_{850}$ response in the dry LBM as well as the observed composite, shown in Figs. 6a and 6c respectively, indicates that the Philippine Sea anticyclone is much stronger than the Southern counterpart, conceivably due to the anomalous cooling located slightly to the north of the equator.

These results are fairly consistent with WWF and clearly show that the anomalous circulation over the western Pacific during ENSO is mainly controlled by the convective activity in the same region but not by the convection anomaly over the central–eastern Pacific which is a direct response to El Niño/La Niña. On the other hand, one may ask whether the suppressed convection over the maritime continent is also an aspect of ENSO. Since the origin of this convective suppression is one of key questions addressed in this study, it is detailed in the following sections.

### *b. Moist LBM experiments*

It is no doubt that the anomalous heating and cooling over the central–eastern Pacific associated with El Niño and La Niña modulate the Walker, as well as Hadley, circulation. Some people discuss that the enhance convection during El Niño brings an eastward shift in the mean Walker circulation entirely and thus weakens convections over the maritime continent where the climatological convective activity is quite strong. However, such an argument has not been proven and even seems crude since there is no justification for why the convection must be preferentially suppressed over the maritime continent no matter how strong the mean

convection is.

An alternative explanation may be led from the low–level momentum balance. If we assume that the mean easterly is not strong enough at lower levels, low-level cyclonic response to the El Niño heating accompanies an equatorward flow to the west, which is balanced by an anomalous surface divergence following the Sverdrup relationship $\beta v = -fD$. This divergence would result in the subsidence strengthened over the off-equatorial western Pacific, therefore may be responsible to suppress convections. In order to test this hypothesis, we look at the $\psi_{850}$ and 500 hPa pressure vertical velocity ($\omega_{500}$) responses in M1 and M1Z, which employs the SST forcing same as M1 but uses the zonally uniform basic state (see Table 1). In M1Z, the low–level cyclonic response extends to the west of the dateline, which in fact accompanies anomalous subsidence in its equatorside. While such a descent suppresses the convection as seen in the negative $< Q_c' >$ response (not shown), it is still far from the maritime continent and furthermore confined to the off–equator. The steady response under the zonally varying basic state of M1 even reveals the cyclonic anomaly and associated descent moved to the east, which is apart enough to affect the western Pacific convections.

It was thus suggested that the SST anomaly in region I (cf. Fig. 3a) *alone* cannot explain the convective suppression over the maritime continent. Another possibility which should be examined is that additional SST anomaly in other regions is necessary to suppress the convections. If this is the case, which region is important? To answer this question, we compared $\psi_{850}$ and $< Q_c' >$ responses in the most LBM experiments between M1, M2 and M3 (see Table 1 for the description). In M2, the SST cooling in the western Pacific (region II) is incorporated into the region I SST anomaly in computing the external forcing while a basin–wide warming in the Indian Ocean (region III) is further included in M3.

The $\psi_{850}$ and $< Q_c' >$ responses in M1 are exactly the same as Figs. 7b and 5c, showing neither the anticyclonic anomalies nor the anomalous convective cooling over the western Pacific (Fig. 8a). When negative SST anomalies are added in the western Pacific (M2, Fig. 8b) negative $< Q_c' >$ response in the northern off-equator extends toward west and a weak anticyclonic

$\psi_{850}$ response appears further to the west although the amplitude is much weaker than the observations. On the other hand, M3 depicts that the additional SST warming in the Indian Ocean drastically changes $< Q_c' >$ hence $\psi_{850}$ response pattern not only aloft but also over the remote western Pacific (Fig. 8c). An anomalous convective cooling over the central equatorial Indian Ocean which has been found in M1 and M2 disappeared in M3, even reversed to a weak heating. Convections over the western Pacific are considerably suppressed as confirmed by anomalous cooling intensified and extended between 120°E and 160°E. They also accompany a narrow band of additional heating straddling northern Australia and Indonesia, which is not found in the observed OLR anomalies (Fig. 6a). As expected from Fig. 6c, anomalous cooling strengthened in M3 has induced the Philippine Sea anticyclone and the southern counterpart with realistic amplitude.

Since M3 is forced by SST anomalies both in the Indian Ocean and western Pacific, a relative importance of these SST anomalies in weakening the convection over the maritime continent is evaluated by taking differences between experiments M1–M3. Shown in Fig. 9a is the difference in $< Q_c' >$ and the 850 hPa wind responses between M1 and M2, which quantifies the impact of SST anomalies in region II while Fig. 9b is the difference between M2 and M3 corresponding to the effect of SST anomalies in region III. Because the model is linear, sum of those difference maps becomes equivalent to the response to SST anomalies in regions II and III. It is shown that the negative $< Q_c' >$ response to the cooling SST in the western Pacific has a minimum around 160°E, which is away eastward by 30 degrees from the center of observed negative OLR anomalies, and so does the anticyclonic response (Fig. 9a). This is again consistent with an AGCM experiment by WWF, showing the anticyclonic response to the western Pacific cooling of SST shifted eastward than expected (cf. their Fig. 13a). The $< Q_c' >$ response to the Indian Ocean warming reveals negative minima in the off–equatorial western Pacific around 130°E, which is closer to observations (Fig. 9b). While $< Q_c' >$ in Fig. 9b has some deficiencies such as unrealistic heating anomaly around 110°E and the western Pacific cooling anomaly split into two off–equatorial minima unlike the observed OLR composite, the comparison with Fig. 9a

indicates that the Indian Ocean SST anomalies affect the convection and circulation anomalies over the western Pacific as much as or stronger than the local SST cooling.

As mentioned in the introduction, the Philippine Sea anticyclone is associated with the northward advection of warm air that contributes to the warmer winter over East Asia during El Niño. Such a situation is clearly identified in the ENSO composite for observed temperature and wind anomalies at 850 hPa (Fig. 10a). Along the northwestern edge of the anticyclonic anomalies there is a strong southwesterly which is in phase with the warmest temperature anomaly. The moist LBM captures some of these low–level anomalies when forced by SST anomalies in the whole tropical Pacific and Indian Ocean basins, i.e., M3 (Fig. 10b). The position of southwesterly coincides with the maximum temperature response as in observations while they are slightly shifted southward. Note that the warm temperature anomaly in Fig. 10a covers most of East Asia of eastern China, Korea and Japan while that diagnosed in the model is confined to the south of 30°N and even cooling response dominates to the north, suggesting that the effect of tropical SST forcing can reach the subtropics but not midlatitude over East Asia.

A significant impact of the Indian Ocean warming in suppressing the western Pacific convections can be interpreted in terms of changes in the Walker circulation. To understand it, we showed in Fig. 11 the equatorial (10°S–10°N) vertical wind ($\omega$) responses in M1 and M3 together with the corresponding SST anomaly. In M1, the $\omega$ response depicts large negative values in the eastern Pacific where the positive SST anomaly is given (Fig. 11a). This strong ascending motion is compensated by weak descent in all the rest longitudes. The subsidence is especially strong to the east of ascent. This is reasonable since the anomalous vertical motion associated with a Gill–like response will dominate to the east (west) of heating in the equatorial band (off–equator) in association with the center of a forced Kelvin (Rossby) wave. In M3, in addition to the ascending motion in the eastern Pacific, which remains the same, another ascending branch comes to happen in the Indian Ocean (Fig. 11b). Since the ascending response is largely compensated by a subsidence to the east as in M1, the descent in the western Pacific

is preferably enhanced, which appears to be responsible for the convective suppression found in Fig. 8c.

### *c. Wind–evaporation feedback*

A comparison between M1–M3 indicates the importance of Indian Ocean SST anomalies for the development of the Philippine Sea anticyclone. At the same time it is shown that the local sea surface cooling contributes as well (cf. Fig. 9a). Since the negative SST anomaly is located under the eastern half of the anticyclone, anomalous northeasterly would accelerate trade wind then further cool the ocean surface. This forms a positive wind–evaporation–SST feedback first postulated by WWF, which may explain the persistence of the Philippine Sea anticyclone if it really works. The moist LBM explicitly involves such a feedback as explained in section 2c, so that it will be worth examining whether the positive feedback is at work. For this purpose, another diagnosis was made with the SST forcing as in M3 but without the wind–evaporation feedback terms (M4, see table 1).

Shown in Fig. 12a is the difference in surface wind and the surface diabatic heating responses between M3 and M4, in which the heating is converted to the thermal forcing for SST. The most conspicuous difference in the wind response is found over the northern tropics where an anomalous northeasterly blows though the magnitude is less than half of the actual response in M3. It certainly happens that the northeasterly anomaly strengthens the wind speed in conjunction with the background trade wind, then produces a net cooling for local SSTs through enhanced evaporation. The difference field also shows a positive thermal forcing at the surface along the Southeast Asian coast, which would contribute to bring the SST warming there. The overall pattern in the heating difference shown in Fig. 12a is an east–west dipole in the northern tropical western Pacific, which has some similarity to the SST anomaly pattern that forced steady responses (Fig. 12b). This resemblance reinforces the positive wind–evaporation–SST feedback being a relevant process working in the western Pacific, as proposed by WWF. Simultaneously, however, the $\psi_{850}$ and $< Q_c' >$ responses in M4 reveal the anomalous cooling over the western Pacific and the Philippine Sea anticyclone, both of which are quite similar to

those in M3 (not shown). This implies that the wind–evaporation feedback is not crucial for the development of those anomalies but seems to help them lasting longer time.

# 5 Observational analysis

In the previous section, results of the LBM diagnosis have been presented and compared to observed composites for ENSO. The major finding obtained was that the modest warming of the Indian Ocean may have a considerable impact in setting up the anomalous convection and circulation over the western Pacific. Here we came back to further look at observational data to seek an evidence that supports the above hypothesis.

For that purpose, a lagged composite is made for monthly $\psi_{850}$, $\omega_{500}$ and SST anomalies. The composite is again based on the Niño 3 SST and the lag is taken for each 1yr before and after the mature January of El Niño/La Niña. Figure 13a depicts a time series of the lagged composite anomaly for $\psi_{850}$ averaged over 100°–140°E and 0°–20°N which covers the Philippine Sea anticyclone (see the map shown in the top right). As noted by Harrison and Larkin (1996) and WWF, the Philippine Sea anticyclone rapidly develops around October then persists beyond the next spring with decaying gradually (Fig. 13a). It is interesting to compare this evolution with the $\omega_{500}$ anomaly obtained in a similar manner but averaged over the western Indian Ocean (Fig. 13b). The $\omega_{500}$ anomaly keeps positive value until October before the El Niño mature season then changes the sign to negative, lasting into next February. The transition from positive to negative anomaly, corresponding to the reversal from descent to ascent, appears as rapid as that in $\psi_{850}$. This coherent development of the anticyclonic and ascending anomalies suggests the relevance of our hypothesis referred to at the beginning of this section. On the other hand, the positive $\psi_{850}$ anomaly exists even after the negative $\omega_{500}$ anomaly was decayed. This is also reasonable when we interpret such a persistence as a result from the positive atmosphere–ocean feedback in the western Pacific as described by WWF and in section 4c.

Considering the $\omega$ response in M1 and M3 (cf. Fig. 11) and the observed time evolution shown in Fig. 13, we speculate that the Indian Ocean warming occurred around October. To verify it, the lagged composites for $\omega_{500}$ and SST anomalies averaged in the equatorial strip (10°S–10°N) are plotted in Fig. 14. Over the central Pacific, an anomalous ascending motion starts developing around April of Yr(0) (i.e. the year before mature El Niño) concurrent with the SST warming associated with El Niño. In the Indian Ocean, however, SST anomaly during this period is quite weak, then gradually develops around October. As indicated in Fig. 13b, $\omega_{500}$ anomaly rapidly changes the sign over the western Indian Ocean in October (Fig. 14a), which corresponds to the time when the underlying SST anomaly reaches +0.5 K. The El Niño SST anomaly still grows after October of Yr(0) while the Indian Ocean SST anomaly retains nearly the same magnitude (Fig. 14b). The lagged warming of the Indian Ocean as seen in Fig. 14b has already been reported by many researchers and the mechanism is discussed as well (Klein et al. 1999; Lau and Nath 2000), which is beyond the scope of this study. It should be noted that the evolution of the Indian Ocean SST anomaly is smoother than that of $\omega_{500}$ anomaly which shows much rapid transition, suggesting that nonlinearity between convection and SST has a role, namely, convections over the Indian Ocean may suddenly become active when SST exceeds a certain threshold as postulated by Gadjil et al. (1984) and Graham and Barnett (1987). Such a possibility should be kept in mind although we cannot discuss it further at this moment.

The lagged composites shown in Fig. 14 supports our thought that the delayed warming of the Indian Ocean seems to explain the development of the anomalous ascending motion aloft hence the Philippine Sea anticyclone both taking place in October. This also implies that M1 (or M2) and M3 presented in section 4 roughly correspond to the situation before and after October of Yr(0). Figure 14 gives another suggestion that further supports our idea. The western Pacific SST starts cooling around April of yr(0), roughly the same time as the eastern Pacific warming although the former reaches the peak earlier than the latter. This is not surprise because the cooling signal is probably a part of El Niño itself (Wang et al. 1999).

On the other hand, the corresponding $\omega_{500}$ anomaly is yet weak in that period even though it does exits, then rapidly intensified around October which is again in phase with the reversal in the Indian Ocean $\omega_{500}$ anomaly.

# 6 Summary and discussion

We have developed a novel type of the linear baroclinic model which coupled the dynamics with active cumulus convection and surface heat fluxes, called the moist LBM in this study. The model solves forced steady response of the coupled dynamical–convective system to a prescribed SST anomaly, leading to the response which often accompanies diabatic heating anomalies not only over the SST anomaly but also over remote regions.

Before we discuss model caveats and a possible direction toward which the model is further developed, results of its application to the ENSO teleconnection over the western Pacific are summarized. Particular attention was paid to understand the formation mechanism of the Philippine Sea anticyclone that links El Niño with the Asian winter monsoon. Consistent with WWF, we confirmed using the conventional dry LBM the anticyclonic anomaly interpreted as a Rossby response to the anomalous diabatic cooling due to suppressed convections over the maritime continent. Then, to clarify why the convections are suppressed over the region we diagnosed the dynamical–convective response in the moist LBM forced by ENSO–related observed SST anomalies in various regions (cf. section 4). We found that Indian Ocean SST anomalies, as well as the SST anomalies in the equatorial Pacific, are relevant in weakening the western Pacific convective activity, as schematically illustrated in Fig. 15.

In the upper panel of Fig. 15, the anomalous Walker circulation revealed in the model response is presented in association with the warming in the eastern equatorial Pacific. As in observations, convections are greatly enhanced over the central tropical Pacific and the resultant heating anomaly excites a pair of low–level cyclonic responses over the subtropics, which accompanies Rossby wave trains toward higher latitude. The anomalous heating is balanced by

a strong upward motion, compensated by a weak subsidence in all the other equatorial regions. Since the circulation response over the midlatitude Pacific and the anomalous descent over the tropics outside of the Pacific are a bi–product of the convective heating anomaly in the central equatorial Pacific, the former is not sensitive to an anomalous diabatic cooling associated with the latter, as described in section 3. The anomalous subsidence also occurs in the western Pacific, however, it does not preferentially suppress convections over the region.

When a modest warming of the Indian Ocean is incorporated into the SST forcing, the response of the Walker circulation as well as the anomalous convection is modified as shown in the bottom panel of Fig. 15. The convective activity is now enhanced over the Indian Ocean though not stronger than that in the central Pacific. It yields another ascending branch in the anomalous Walker cells, in turn reinforcing the subsidence between the two ascents, namely, over the western Pacific. The intensified descent is accompanied by the diabatic cooling anomaly, which then induces the Philippine Sea anticyclone.

Since the Indian Ocean SST starts raising several months behind the development of El Niño, two response patterns illustrated in Fig. 15 can also be interpreted as those in a different phase of the ENSO evolution. Observed composites presented in section 5 show that the rapid development of the Philippine anticyclone is concurrent with a reversal of the vertical motion over the western Indian Ocean both found in October. Thus the anomalous circulation patterns are close to the upper (lower) panel of Fig. 15 before (after) October prior to the El Niño mature. On the other hand, the Indian Ocean warming is perhaps a delayed response to El Niño through changes in the surface net heat flux, in particular the latent heat and shortwave radiation (Klein et al. 1999; Lau and Nath 2000). The shortwave anomaly, i.e. increased solar insolation, is argued to result from a reduction in the cloud cover. This is also coincident with our moist LBM diagnoses M1 and M2 indicating suppressed convection over the tropical Indian Ocean (Figs. 8a and 8b) that ought to result in less convective clouds when the Indian Ocean is yet warming. Considering these arguments, processes presented in Fig. 15 may be regarded as a lagged, remote feedback of the coupled atmosphere–ocean system in the Pacific and Indian

Ocean basins.

Another process which is not emphasized in Fig. 15 is an effect of the weak SST cooling in the western Pacific on the Philippine Sea anticyclone. The sea surface cooling was also capable of suppressing in–situ convections hence forcing the anticyclonic circulation anomalies (cf. Figs. 8b and 9a) which appear to in turn enhance the initial SST anomaly via the positive wind–evaporation feedback. These processes have been depicted by WWF and therefore our results are to reinforce WWF's argument. However, in the present diagnoses the impact of local SST cooling on the western Pacific convection was not as strong as the Indian Ocean warming (Fig. 9) and the positive air–sea feedback seemed not crucial at least for the development of the anomalous convection and circulation over the western Pacific.

Our hypothesis can be verified by hindcast AGCM experiments forced with observed SST anomalies in the Pacific but with and without Indian Ocean SST anomalies. While a number of works have been made to carry out an AMIP–type hindcast run (Kitoh 1992; Ju and Slingo 1995; Sperber and Palmer 1996; Goswami 1998; Meehl and Arblaster 1998), few of them performed an additional AGCM run without Indian Ocean SST anomalies to compare the response fields. Recently, however, Farrara et al. (2000), who examined circulation anomalies during 1997/98 El Niño by means of an AGCM ensemble, showed that the Indian Ocean warming is responsible for a Rossby wave source over Southeast Asia hence significant in affecting the extratropical circulation anomalies during ENSO. Su et al. (2001) also found in their simplified AGCM that the western Pacific convection associated with the 1997/98 El Niño was suppressed by the local cooling and the Indian Ocean warming but not by the strong El Niño warming in the eastern equatorial Pacific. Both of their results are consistent with our hypothesis in terms of the role of Indian Ocean and western Pacific SST anomalies in the ENSO teleconnection. On the other hand, in a series of intriguing GCM experiments to explore the impact of El Niño on the Asian monsoon and the atmosphere–ocean system in the Indian Ocean, Lau and Nath (2000) simulated the Philippine Sea anticyclone realistically even with the tropical Pacific SST anomaly alone. If this has been due to negative SST anomalies in the western Pacific,

the relative impact between Indian Ocean warming and in–situ cooling on the western Pacific convection might be dependent upon model used.

The moist LBM is yet in progress although it already involves the core of diabatic processes. One of caveats in the current moist model is the lack of surface evaporation anomaly over lands as mentioned in section 2c. Because of the small heat capacity, surface temperature $T_s'$ cannot be prescribed over lands hence should be determined via the balance among surface heat budgets. Besides an anomaly of soil wetness is required for the accurate estimate of the anomalous heat fluxes over the land area. A possible way to solve this problem is to couple a simple land surface model with the moist LBM. It may enable us to apply the model to phenomena in which the diabatic heating over continents is of importance such as the Asian summer monsoon.

Another progress will be made by incorporating diabatic heating associated with stratiform clouds into the model. Since the stratus rainfall dominates over the midlatitude ocean, such an extension may provide the moist LBM used to examine the atmospheric response to extratropical SST anomalies. This issue is still a quite attracting problem, but it would additionally necessitate to parameterize feedbacks from transient disturbances as well since previous works suggest the transient eddy feedback of importance in determining the atmospheric response to midlatitude SST forcing (e.g. Peng and Whitaker 1999; Watanabe and Kimoto 2000).

# 7 Concluding remarks

The moist LBM delineated in this study is placed in the first step of advanced application of the linear atmospheric modeling which we aim. In the present paper we used this model to examine the atmospheric teleconnection associated with ENSO, but the model may be applied to wider issues when we include some other physical processes into the LBM as discussed in the previous section. Apart from forced steady problem, an exploration of free modes of the coupled dynamical–convective system will also be an interesting challenge in particular if the moist LBM was coupled to a simple, linear ocean model. Some of these works are currently

ongoing.

The reason why convections are suppressed over the western Pacific during El Niño has been argued such that they are simply a consequence of the eastward shift in the Walker circulation. However, it turned out from the moist LBM diagnoses that the actual processes are not so simple although there is no doubt that El Niño originates them. The mechanism for the convective suppression over the western Pacific may involve the atmosphere–ocean system in the Indian Ocean, and therefore, it suggests that the prediction of East Asian climate associated with ENSO can be improved by means of a coupled model relevant to simulate a coupled atmosphere–ocean response in the Indian Ocean to El Niño. The possibility which we postulate here should be carefully verified.

*Acknowledgments*

We thank M. Kimoto, B. Wang, T. Li, and Y.-Y. Hayashi for stimulating discussion. Most of this work was completed while MW was at University of Hawaii. This work is partially supported by a Grant–in–Aid for Scientific Research from the Ministry of Education, Science, and Culture of Japan. FFJ is also supported by NOAA grants GC01–229.

# References


Betts, A. K., 1986: A new convective adjustment scheme. Part I: Observational and theoretical basis. *Quart.J.R.Met.Soc.*, **112**, 677–691.

Betts, A. K., and M. J. Miller, 1986: A new convective adjustment scheme. Part II: Single column tests using GATE wave, BOMEX, ATEX and arctic air–mass data sets. *Quart.J.R.Met.Soc.*, **112**, 693–709.

Branstator, G., 1985: Analysis of general circulation model sea–surface temperature anomaly simulations using a linear model. Part I: Forced solutions. *J.Atmos.Sci.*, **42**, 2225–2241.

Brown, R. G., and C. S. Bretherton, 1995: Tropical wave instabilities: Convective interaction with dynamics using the Emanuel convective parameterization. *J.Atmos.Sci.*, **52**, 67–82.

Chang, C. P., and H. Lim, 1988: Kelvin wave–CISK. A possible mechanism for the 30–50 day oscillation. *J.Atmos.Sci.*, **45**, 1709–1720.

Crum, F. X., and D. E. Stevens, 1983: A comparison of two cumulus parameterization schemes in a linear model of wave–CISK. *J.Atmos.Sci.*, **40**, 2671–2688.

Farrara, J. D., C. R. Mechoso, and A. W. Robertson, 2000: Ensembles of AGCM two–tier predictions and simulations of the circulation anomalies during winter 1997–98. *Mon.Wea.Rev.*, **128**, 3589–3603.

Gadjil, S., P. V. Joseph, and N. V. Joshi, 1984: Ocean–atmosphere coupling over monsoon regions. *Nature*, **312**, 141–143.

Gill, A. E., 1980: Some simple solutions for heat–induced tropical circulation. *Quart.J.R.Met.Soc.*, **106**, 447–462.

Goswami, B. N., 1998: Interannual variations of Indian summer monsoon in a GCM: External conditions versus internal feedbacks. *J.Climate*, **11**, 501–522.

Graham, N. E., and T. P. Barnett, 1987: Sea surface temperature, surface wind divergence, and convection over tropical oceans. *Science*, **238**, 657–659.

Hall, N. M., and P. D. Sardeshmukh, 1998: Is the time–mean Northern Hemisphere flow baroclinically unstable? *J.Atmos. Sci.*, **55**, 41–56.

Harrison, D. E., and N. K. Larkin, 1996: The COADS sea level pressure signal: A near–global El Niño composite and time series view, 1946–1993. *J.Climate*, **9**, 3025–3055.

Hayashi, Y., 1970: A theory of large–scale equatorial waves generated by condensation heat and accelerating the zonal wind. *J.Meteor.Soc.Japan*, **48**, 140–160.

Held, I. M., S. W. Lyons, and S. Nigam, 1989: Transients and the extratropical response to El Niño. *J.Atmos.Sci.*, **46**, 163–174.

Hoerling, M. P., and M. Ting, 1994: Organization of extratropical transients during El Niño. *J.Climate*, **7**, 745–766.

Horel, J. D., and J. M. Wallace, 1981: Planetary–scale atmospheric phenomena associated with the southern oscillation. *Mon.Wea.Rev.*, **109**, 813–829.

Hoskins, B. J., and D. J. Karoly, 1981: The steady linear response of a spherical atmosphere to thermal and orographical forcing. *J.Atmos.Sci.*, **38**, 1179–1196.

Ju, J., and J. Slingo, 1995: The Asian summer monsoon and ENSO. *Quart.J.R.Met.Soc.*, **121**, 1133–1168.

Kalnay, E., and co–authors, 1996: The NCEP/NCAR 40–year reanalysis project. *Bull.Amer.Meteor.Soc.*, **77**, 437–471.

Kitoh, A., 1992: Simulated interannual variations of Indo-Australian monsoons. *J.Meteor.Soc.Japan*, **70**, 563–583.

Klein, S. A., B. J. Soden, and N.-C. Lau, 1999: Remote sea surface temperature variations during ENSO: Evidence for a tropical atmospheric bridge. *J.Climate*, **12**, 917–931.

Lanzante, J. R., 1996: Lag relationships involving tropical SSTs. *J.Climate*, **9**, 2568–2578.

Lau, K.-M., and L. Peng, 1987: Origin of low–frequency (intraseasonal) oscillations in the tropical atmosphere. Part I: Basic theory. *J.Atmos.Sci.*, **44**, 950–972.

Lau, N.-C., and M. J. Nath, 2000: Impact of ENSO on the variability of the Asian–Australian monsoons as simulated in GCM experiments. *J.Climate*, **13**, 4287–4309.

Liebmann, B., and C. A. Smith, 1996: Description of a complete (interpolated) outgoing longwave radiation dataset. *Bull.Amer.Meteor.Soc.*, **77**, 1275–1277.

Lindzen, R., 1974: Wave–CISK in the tropics. *J.Atmos.Sci.*, **31**, 156–179.

Louis, J., 1979: A parametric model of vertical eddy fluxes in the atmosphere. *Bound.Layer Meteor.*, **17**, 187–202.

Manabe, S., and R. F. Strickler, 1964: Thermal equilibrium of the atmosphere with a convective adjustment. *J.Atmos.Sci.*, **21**, 361–385.

Meehl, G. A., and J. M. Arblaster, 1998: The Asian–Australian monsoon and El Niño– Southern Oscillation in the NCAR Climate System Model. *J.Climate*, **11**, 1356–1385.

Neelin, J. D., and J.-Y. Yu, 1994: Modes of tropical variability under convective adjustment and the Madden–Julian oscillation. Part I: Analytical theory. *J.Atmos.Sci.*, **51**, 1876–1894.

Nigam, S., 1994: On the dynamical basis for the Asian summer monsoon rainfall–El Niño relationship. *J.Climate*, **7**, 1750–1771.

Parker, D. E., C. K. Folland, A. Bevan, M. N. Ward, M. Jackson, and K. Maskell, 1995: Marine surface data for analysis of climatic fluctuations on interannual to century timescales. *Natural climate variability on decade to century time scales* D.G.Martinson, K.Bryan, M.Ghil,

M.M.Hall, T.R.Karl, E.S.Sarachik, S.Soroostian and L.D.Talley, Eds., National Academy Press, 241–250.

Peng, S., and J. S. Whitaker, 1999: Mechanisms determining the atmospheric response to midlatitude SST anomalies. *J.Climate*, **12**, 1393–1408.

Reed, R. J., and E. E. Recker, 1971: Structure and properties of synoptic–scale wave disturbances in the equatorial western Pacific. *J.Atmos.Sci.*, **28**, 1117–1133.

Sperber, K. R., and T. N. Palmer, 1996: Interannual tropical rainfall variability in general circulation model simulations associated with the Atmospheric Model Intercomparison Project. *J.Climate*, **9**, 2727–2750.

Stark, T. E., 1976: Wave–CISK and cumulus parameterization. *J.Atmos.Sci.*, **33**, 2383–2391.

Stevens, D. E., and R. Lindzen, 1978: Tropical wave–CISK with a moisture budget and cumulus friction. *J.Atmos.Sci.*, **35**, 940–961.

Su, H., J. D. Neelin, and C. Chou, 2001: Tropical teleconnection and local response to SST anomalies during the 1997–1998 El Niño. *J.Geophys.Res.*, **106**, 20025–20043.

Sui, C.-H., and K.-M. Lau, 1989: Origin of low–frequency (intraseasonal) oscillations in the tropical atmosphere. Part II: Structure and propagation of mobile wave–CISK modes and their modification by lower boundary forcings. *J.Atmos.Sci.*, **46**, 37–56.

Tourre, Y. M., and W. B. White, 1995: ENSO signals in global upper–ocean temperature. *J.Phys.Oceanogr.*, **25**, 1317–1332.

Wang, B., R. W. Wu, and X. Fu, 2000: Pacific–East Asian teleconnection: How does ENSO affect East Asian climate? *J.Climate*, **13**, 1517–1536.

Wang, C., R. H. Weisberg, and J. I. Virmani, 1999: Western Pacific interannual variability associated with the El Niño–Southern Oscillation. *J.Geophys.Res.*, **104**, 5131–5149.

Watanabe, M., and M. Kimoto, 2000: Atmosphere–ocean thermal coupling in the North Atlantic: A positive feedback. *Quart.J.R.Met.Soc.*, **126**, 3343–3369.

Watanabe, M., and M. Kimoto, 2001: Corrigendum. *Quart.J.R.Met.Soc.*, **127**, 733–734.

Webster, P. J., V. O. M. na, T. N. Palmer, J. Shukla, R. A. Tomas, M. Yanai, and T. Yasunari, 1998: Monsoons: Processes, predictability, and prospects for prediction. *J.Geophys.Res.*, **103**, 14451–14510.

Xie, S. P., and S. G. H. Philander, 1994: A coupled ocean–atmosphere model of relevance to the ITCZ in the eastern Pacific. *Tellus*, **46**, 340–350.

Yamasaki, M., 1969: Large–scale disturbances in a conditionally unstable atmospherein low latitudes. *Papers Meteor.Geophys.*, **20**, 289–336.

Yu, J.-Y., and J. D. Neelin, 1994: Modes of tropical variability under convective adjustment and the Madden–Julian Oscillation. Part II: Numerical results. *J.Atmos.Sci.*, **51**, 1895–1914.

## Figure captions

**Table 1** Description of moist LBM experiments. The zonally varying basic state is denoted as 3D whereas its zonal average is indicated by ZM.

**Fig.1** Vertical profiles of (a) $A(\sigma)$ and (b) $B(\sigma)$ along 180°E, as a function of the winter basic state. The contour interval is 0.05 and the shading denotes values greater than 0.5.

**Fig.2** (a) Basic state CAPE and (b) the convective efficiency $e_c$ derived from CAPE. The contour interval is 1000 J kg$^{-1}$ and 0.2, respectively, with a supplemental contour of 0.1 in (b). Shading denotes $e_c$ greater than 0.8.

**Fig.3** Composite differences between El Niños and La Niñas for observed winter (a) SST, (b) OLR, and (c) 500 hPa height anomalies. The contour intervals are 0.5 K, 15 W m$^{-2}$, and 20 m, respectively. Anomalies significant at 95% level are shaded. Thick black borders in (a) indicate the area division for moist LBM experiments (see Table 2).

**Fig.4** (a) Scatter plot of observed OLR anomalies against SST anomalies over the central–eastern equatorial Pacific (170°E–90°W, 10°S–10°N). Composites for El Niño, La Niña, and the difference are indicated by red, blue, and orange dots, respectively. (b) As in (a), but for $< Q_c' >$ diagnosed in the moist LBM against given SST anomalies. Note that the axis for OLR is reversed for comparison with $< Q_c' >$.

**Fig.5** (a) Vertically averaged heating, $< Q_c' >$, given to the dry LBM and (b) steady 500 hPa height response to the heating. (c)–(d) $< Q_c' >$ and 500 hPa height responses in the moist LBM to SST anomalies in the region I (M1). The contour interval is 1 K day$^{-1}$ for (a) and (c) while 20 m for (b) and (d). The shading in (c) denotes $< Q_c' >$ less than -0.5 K day$^{-1}$.

**Fig.6** (a) As in Fig. 3, but for $\psi_{850}$ (contour) and OLR (colors in W m$^{-2}$). (b) Steady $\psi_{850}$ response in the dry LBM to the prescribed heating over the eastern equatorial Pacific.

The color shading denotes $< Q_c' >$ in K day$^{-1}$. (c) As in (b), but for the response to the cooling over the maritime continent added to the heating in (b). The same contour interval of $2 \times 10^6$ m$^2$ s$^{-1}$ is used for (a)–(c).

**Fig.7** Steady $\psi_{850}$ and $\omega_{500}$ responses (black and white contours) in the moist LBM to SST anomalies in the region I under the (a) zonally uniform and (b) zonally varying (M1, see Table 2) basic states. The contour interval is $2 \times 10^6$ m$^2$ s$^{-1}$ and $5 \times 10^{-4}$ hPa s$^{-1}$, with shading for $\mid \omega_{500} \mid$ greater than $2 \times 10^{-4}$ hPa s$^{-1}$

**Fig.8** Steady $\psi_{850}$ (contour) and $< Q_c' >$ (colors, in K day$^{-1}$) responses in the moist LBM (a) M1, (b) M2, and (c) M3. The contour interval is $2 \times 10^6$ m$^2$ s$^{-1}$.

**Fig.9** As in Fig. 8, but for differences in $< Q_c' >$ (contour) and the 850 hPa wind (vector) between (a) M1 and M2, and (b) M2 and M3. The contour interval is 0.5 K day$^{-1}$.

**Fig.10** (a) ENSO composite anomalies in temperature (contour) and wind (vector) at 850 hPa calculated as in Fig. 3. The contour interval is 0.5 K. (b) As in (a), but for the steady response in M3.

**Fig.11** Steady $\omega$ response over the equatorial strip (10°S–10°N) in (a) M1 and (b) M3. The contour interval is $2 \times 10^{-4}$ hPa s$^{-1}$ and the descending area is shaded. SST forcing averaged over the same strip is also shown at the bottom of each panel.

**Fig.12** Difference in wind (vector) and diabatic heating (contour) at the surface, between steady responses with and without the wind–evaporation feedback (M3–M4). The heating is converted to the thermal forcing for the ocean, with the contour interval 25 W m$^{-2}$. (b) SST forcing to M3 and M4, the contour interval 0.2 K.

**Fig.13** Lagged composite (difference between El Niños and La Niñas) based on the Niño 3 SST index for observed (a) $\psi_{850}$ over 100°–140°E, 0°–20°N and (b) $\omega_{500}$ over 40°–80°E, 10°S–10°N. Regions for the spatial average are shown in the top–right panel.

**Fig.14** As in Fig. 13, but for (a) $\omega_{500}$ and (b) SST anomalies both averaged over 10°S–10°N. The contour interval is $1 \times 10^{-4}$ hPa $s^{-1}$ and 0.5 K, the shading indicating ascending in (a) and SST anomalies greater (less) than +0.5 (-0.5) K in (b), respectively.

**Fig.15** Schematic diagrams showing the role of Indian Ocean SST anomalies for the Philippine Sea anticyclone. Gray arrows and circles represent the anomalous Walker circulation and the low–level circulation without (upper) and with (lower) the Indian Ocean warming. The symbol $Q$ denotes the anomalous convective heating.

Table 1. Description of moist LBM experiments

| abbreviation | SST forcing | basic state | wind–evaporation feedback |
|---|---|---|---|
| M1 | region I | 3D | on |
| M1Z | region I | ZM | on |
| M2 | region I+II | 3D | on |
| M3 | region I+II+III | 3D | on |
| M4 | region I+II+III | 3D | off |

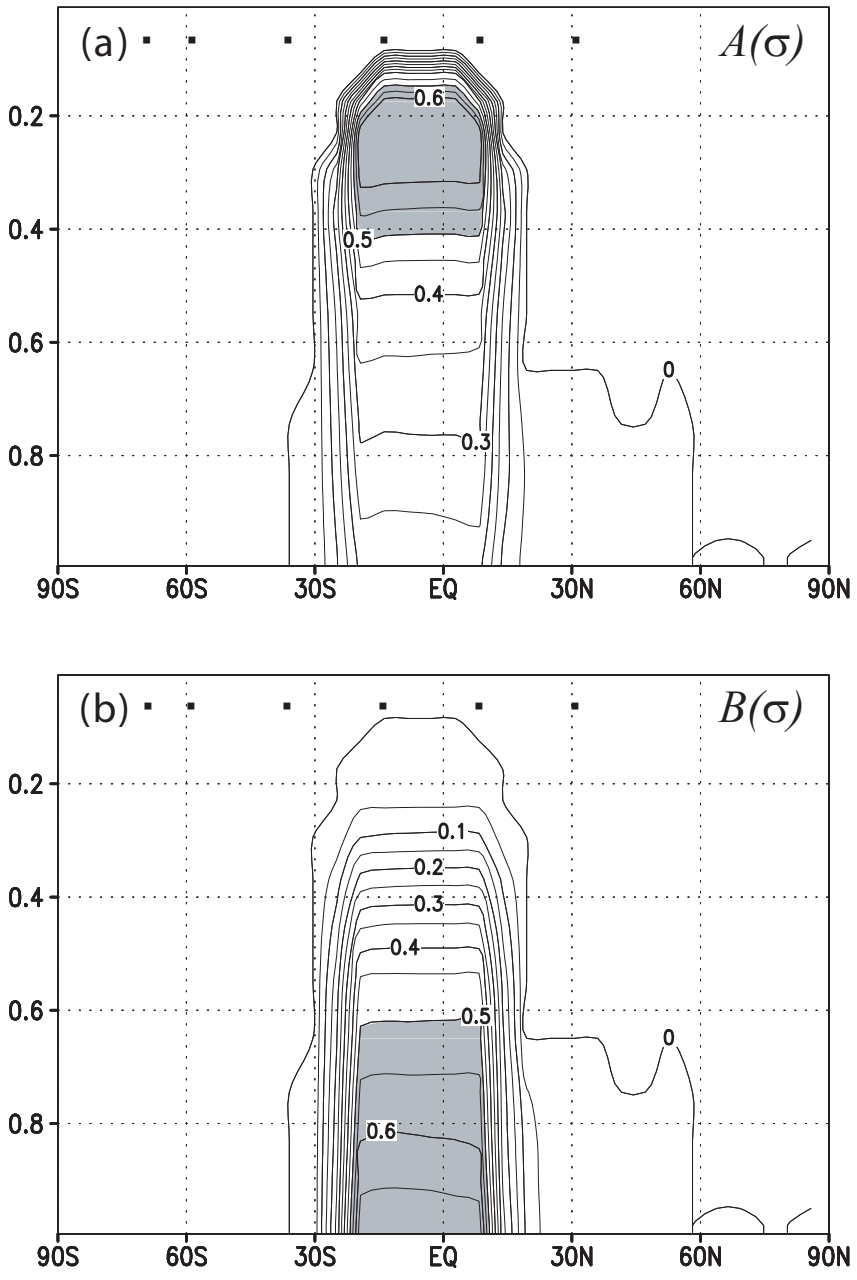
(a)
A(σ)
0.6
0.5
0.4
0
0.3
0.2
0.4
0.6
0.8
90S
60S
30S
EQ
30N
60N
90N
(b)
B(σ)
0.1
0.2
0.3
0.4
0.5
0
0.6
0.2
0.4
0.6
0.8
90S
60S
30S
EQ
30N
60N
90N

Figure 1.

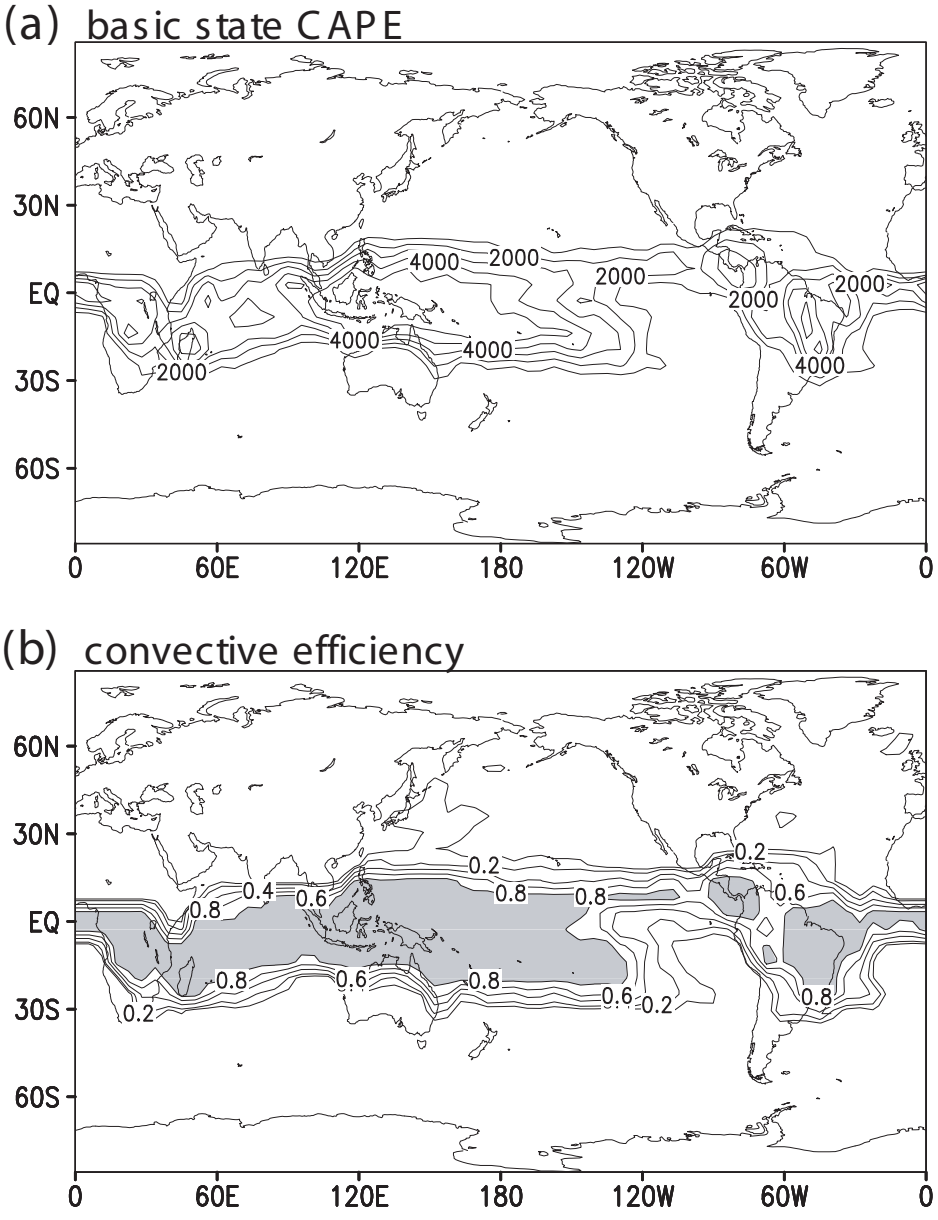
(a) basic state CAPE
60N
30N
EQ
30S
60S
0
60E
120E
180
120W
60W
0
4000
2000
2000
2000
2000
4000
4000
4000
2000
(b) convective efficiency
60N
30N
EQ
30S
60S
0
60E
120E
180
120W
60W
0
0.2
0.2
0.4
0.6
0.8
0.8
0.8
0.6
0.8
0.6
0.8
0.6
0.2
0.2
0.8

Figure 2.

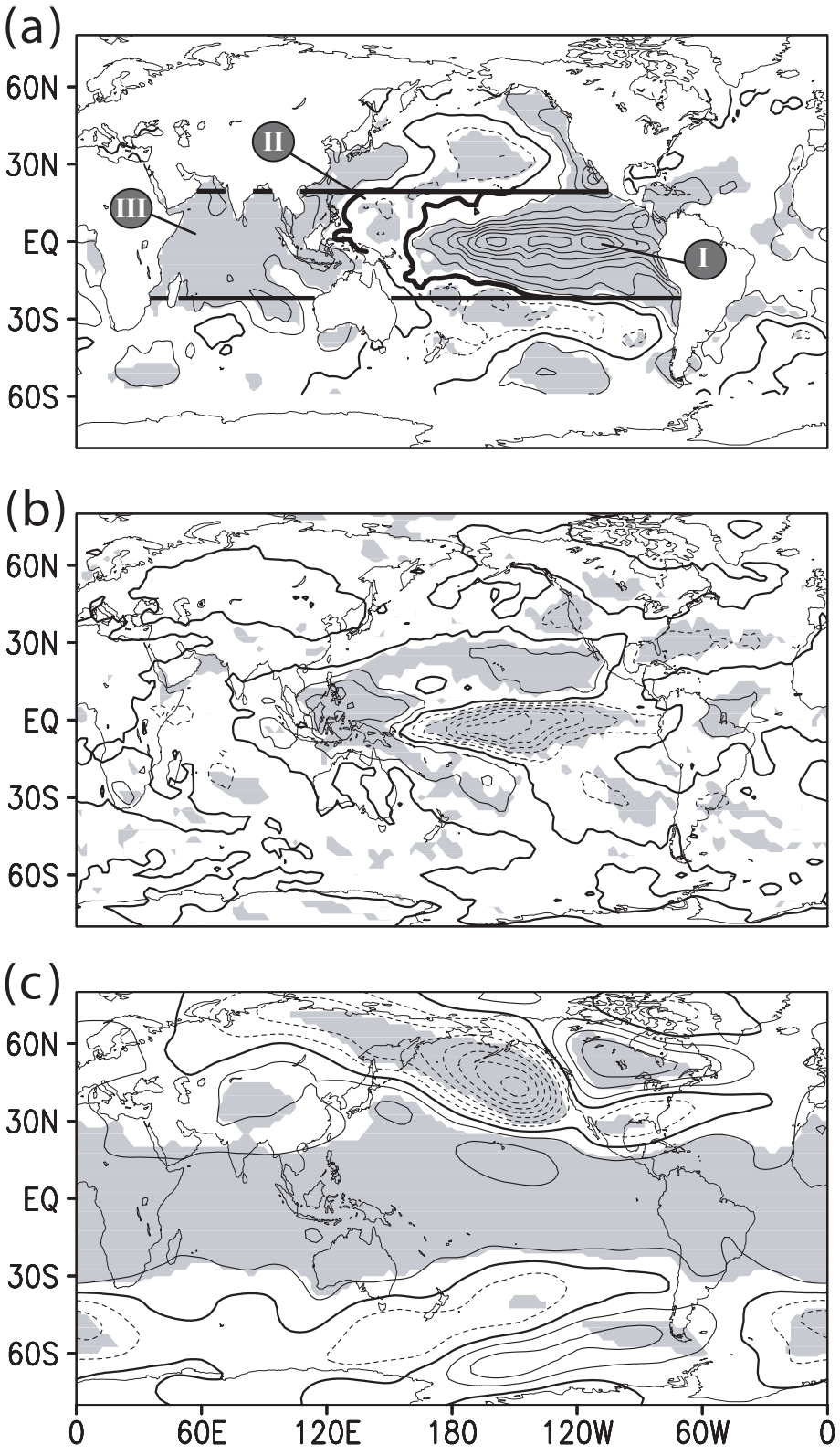
(a)
60N
30N
EQ
30S
60S
II
III
I
(b)
60N
30N
EQ
30S
60S
(c)
60N
30N
EQ
30S
60S
0
60E
120E
180
120W
60W
0

Figure 3.

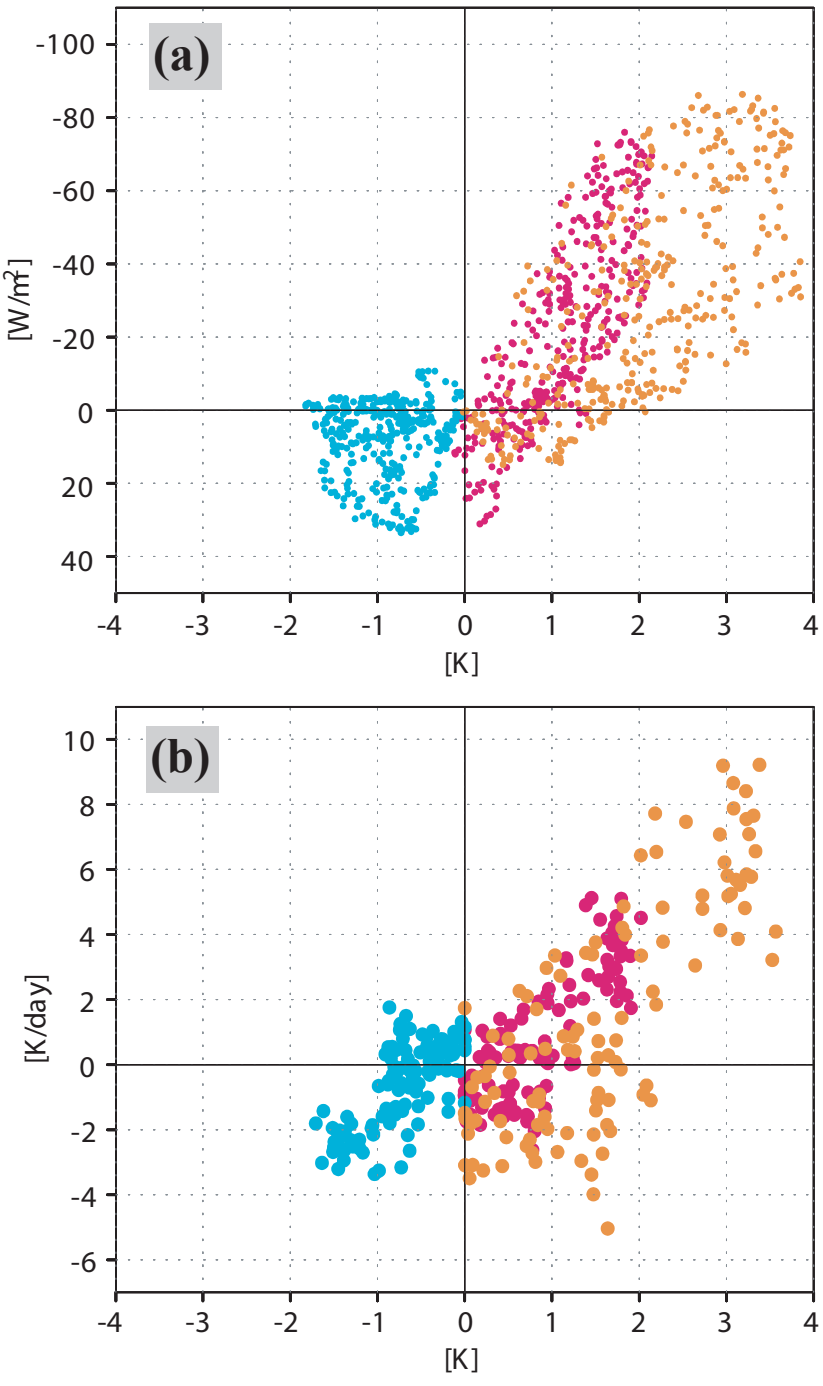
(a)
-100
-80
-60
-40
-20
0
20
40
[W/m²]
-4
-3
-2
-1
0
1
2
3
4
[K]
(b)
10
8
6
4
2
0
-2
-4
-6
[K/day]
-4
-3
-2
-1
0
1
2
3
4
[K]

Figure 4.

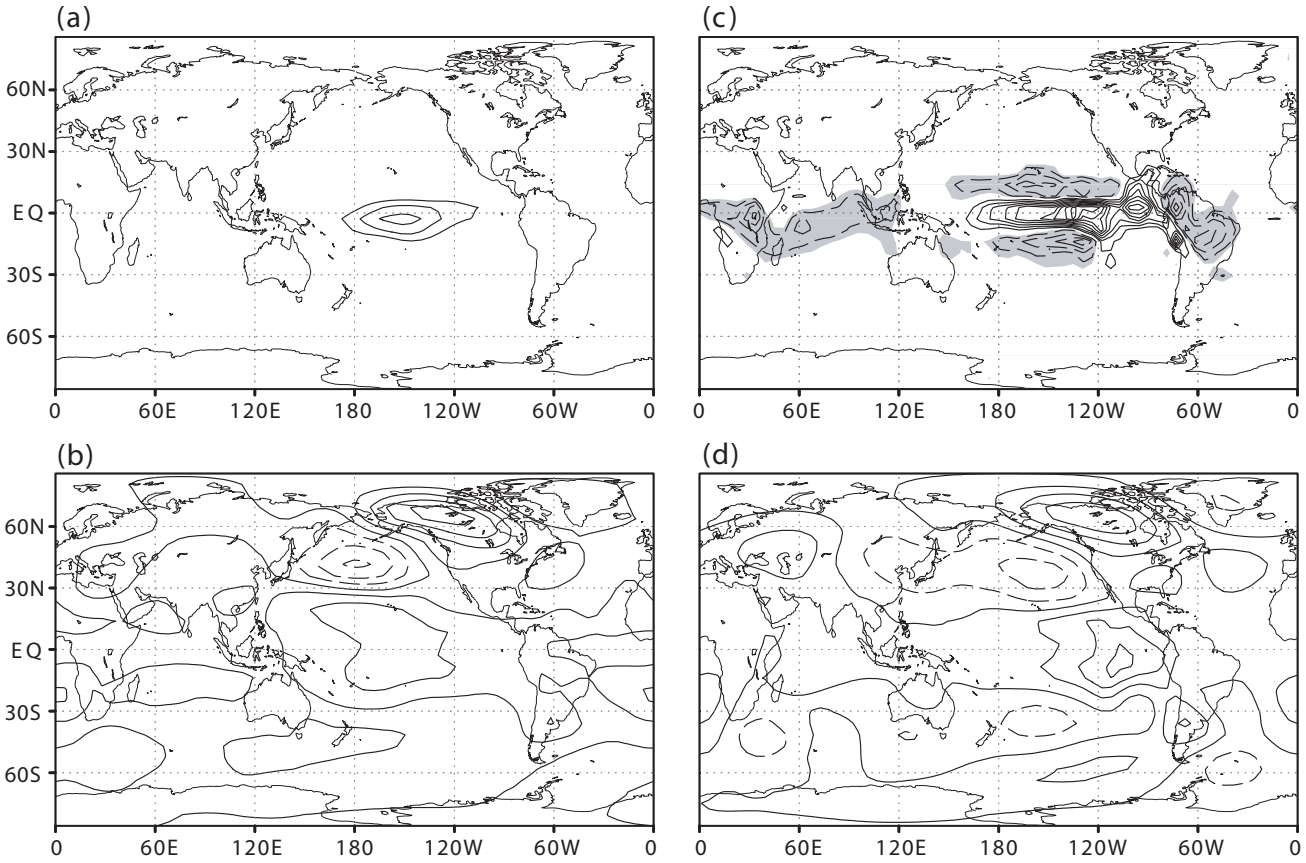


Figure 5.

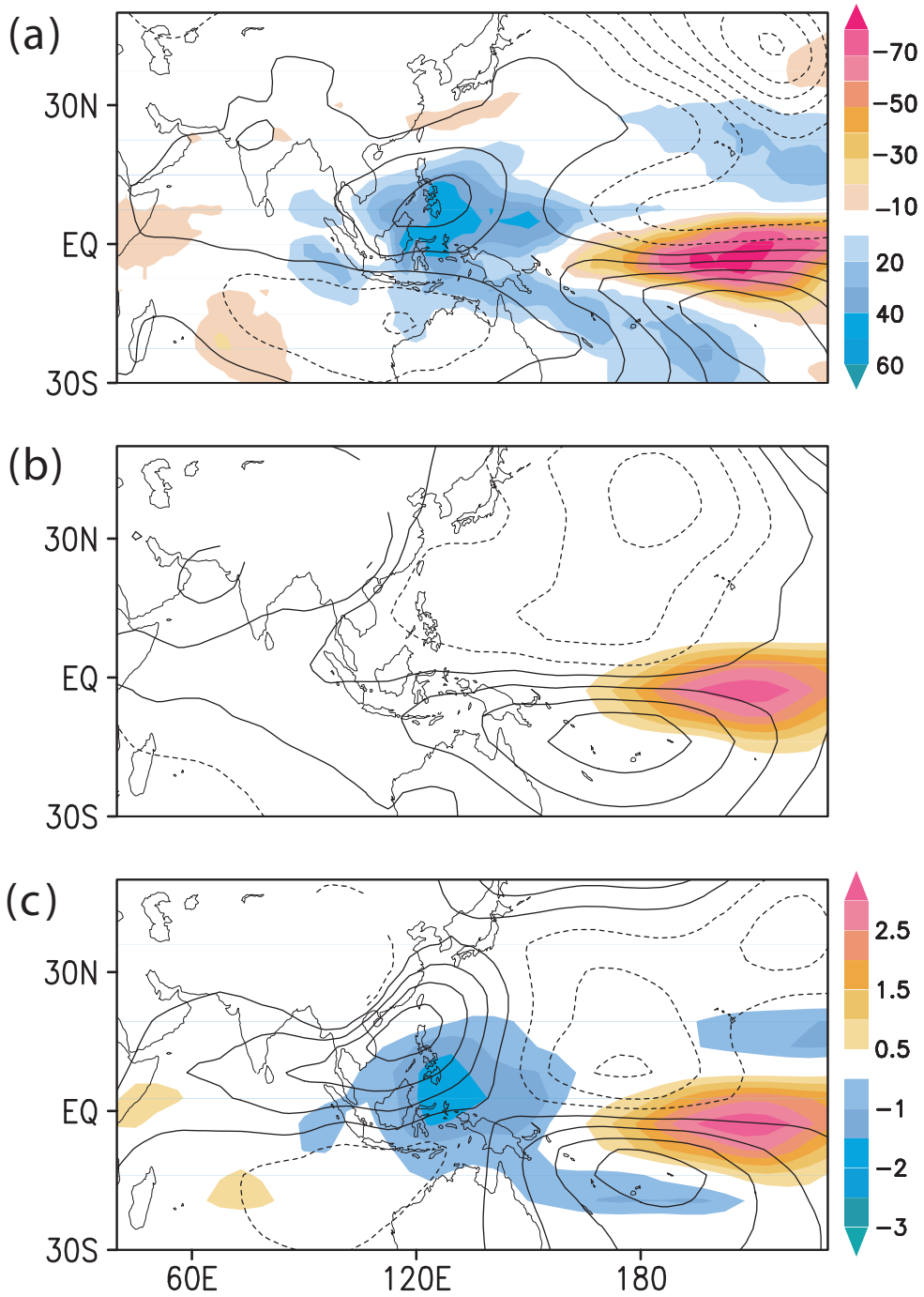
(a)
30N
EQ
30S
−70
−50
−30
−10
20
40
60
(b)
30N
EQ
30S
(c)
30N
EQ
30S
2.5
1.5
0.5
−1
−2
−3
60E
120E
180

Figure 6.

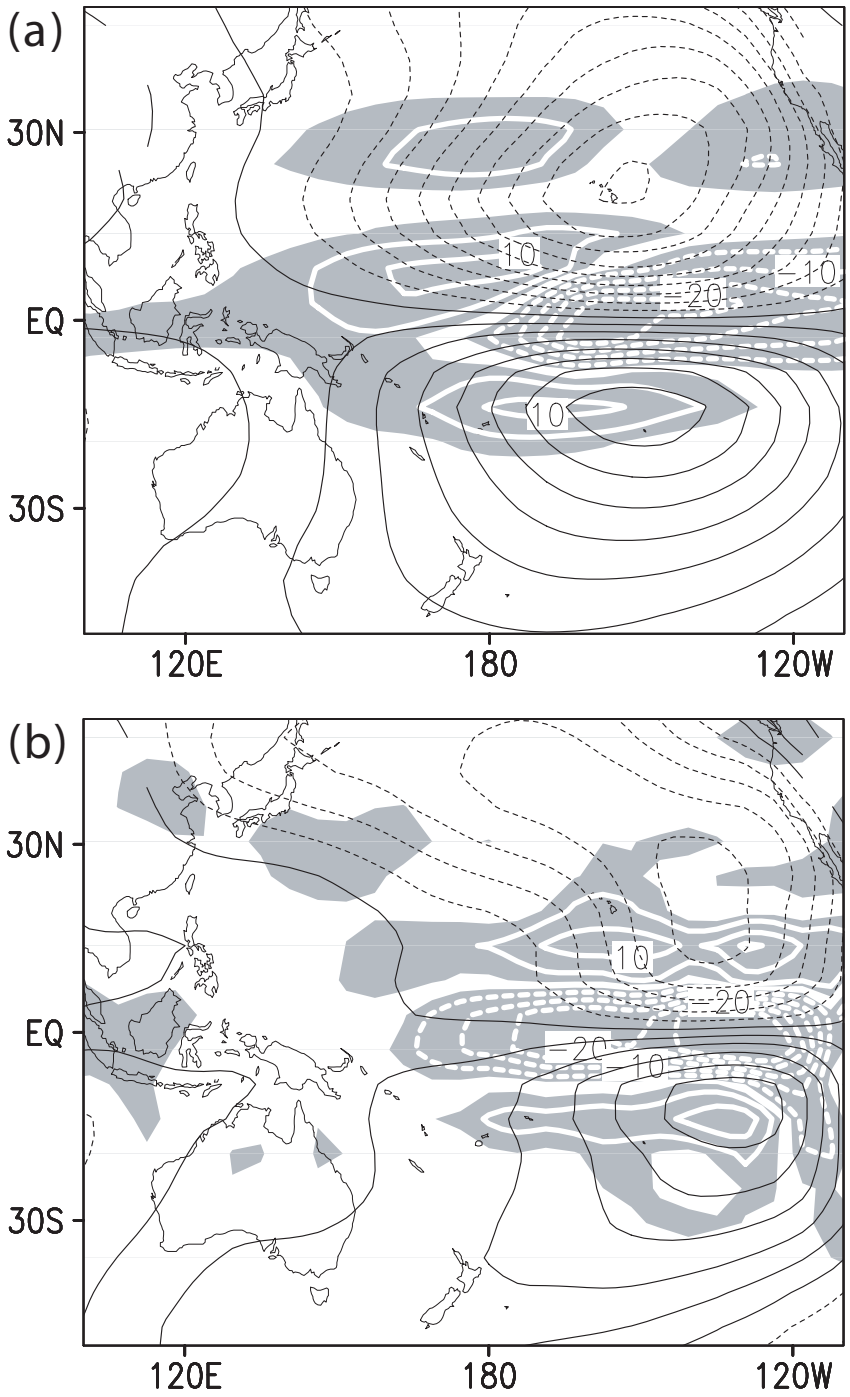
(a)
30N
EQ
30S
120E
180
120W
10
-10
-20
10
(b)
30N
EQ
30S
120E
180
120W
10
-20
-20
-10

Figure 7.

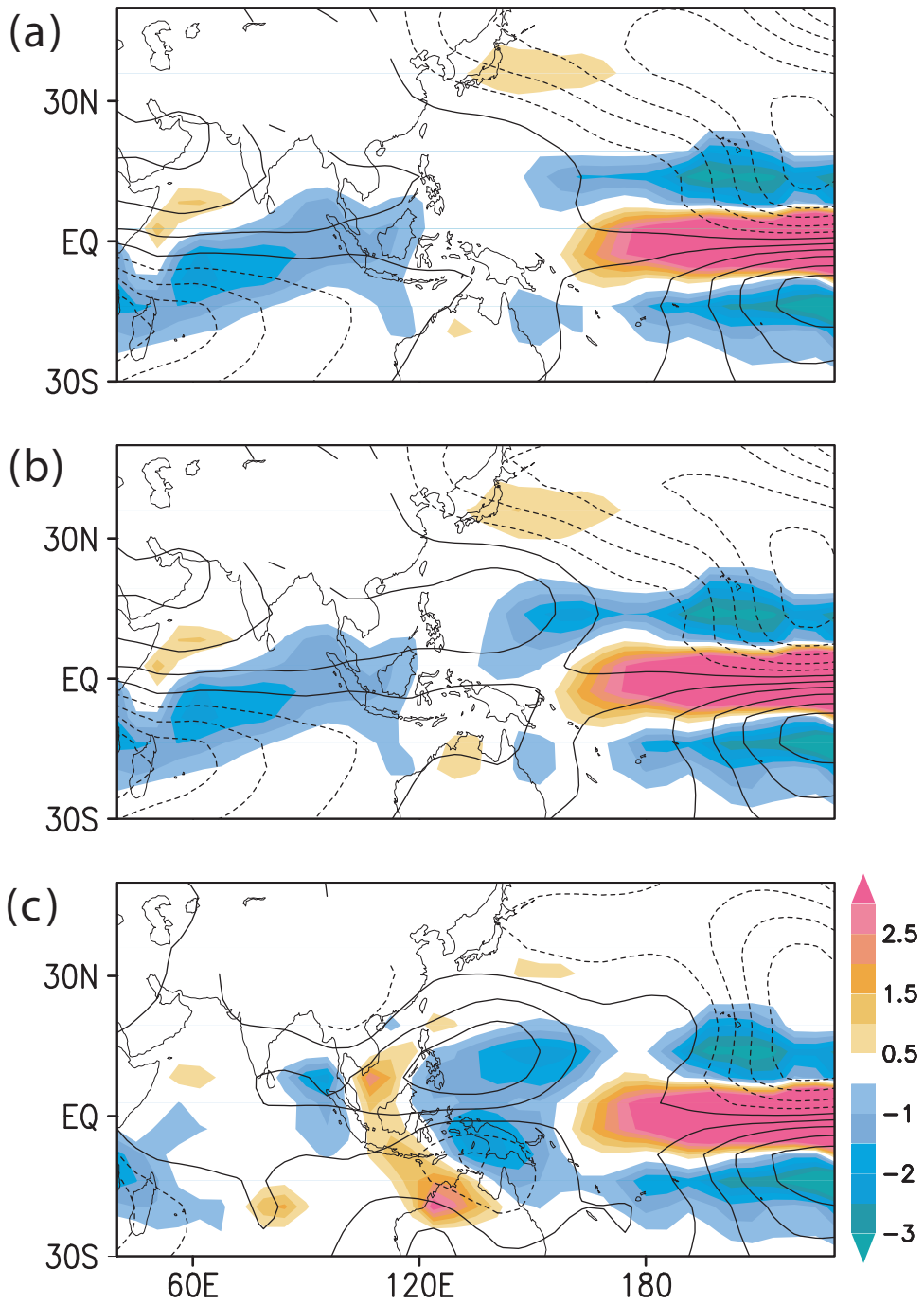


Figure 8.

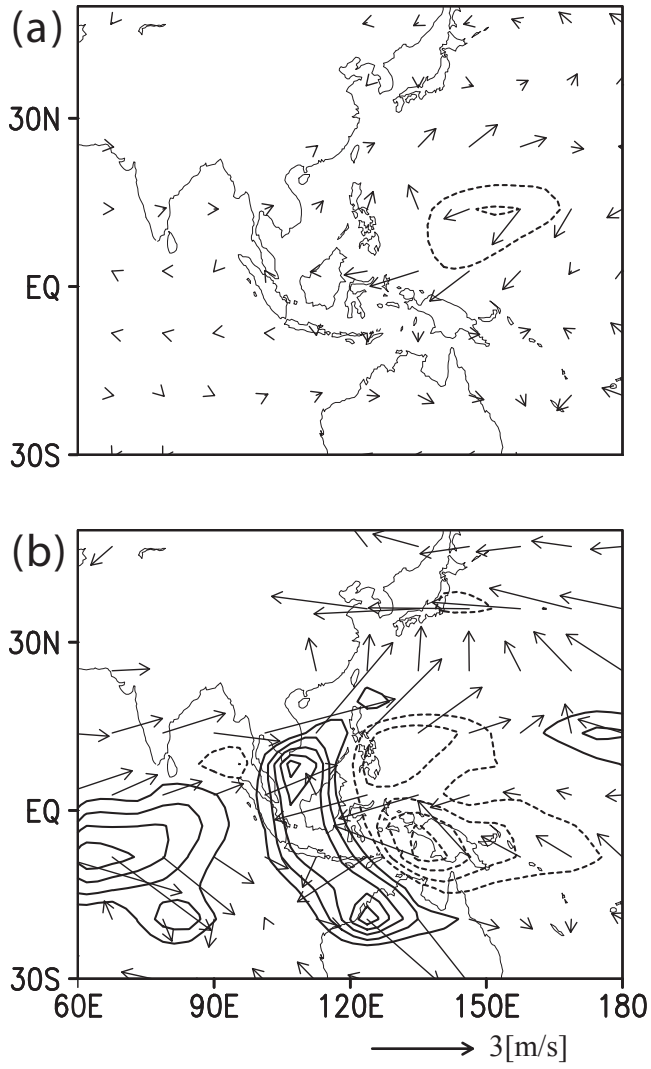


Figure 9.

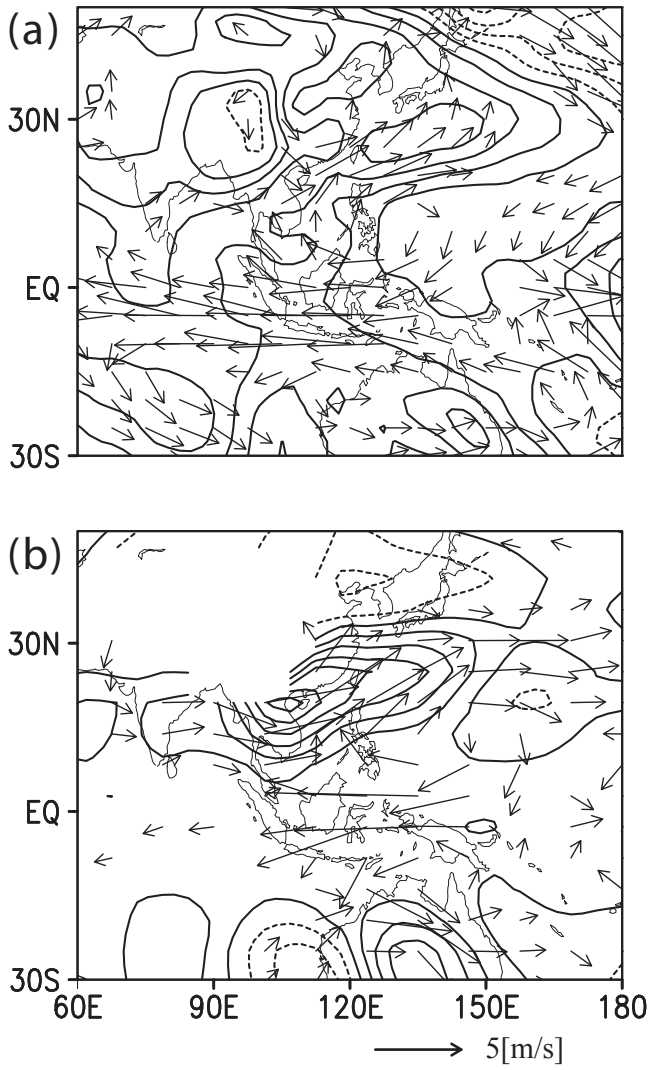


Figure 10.

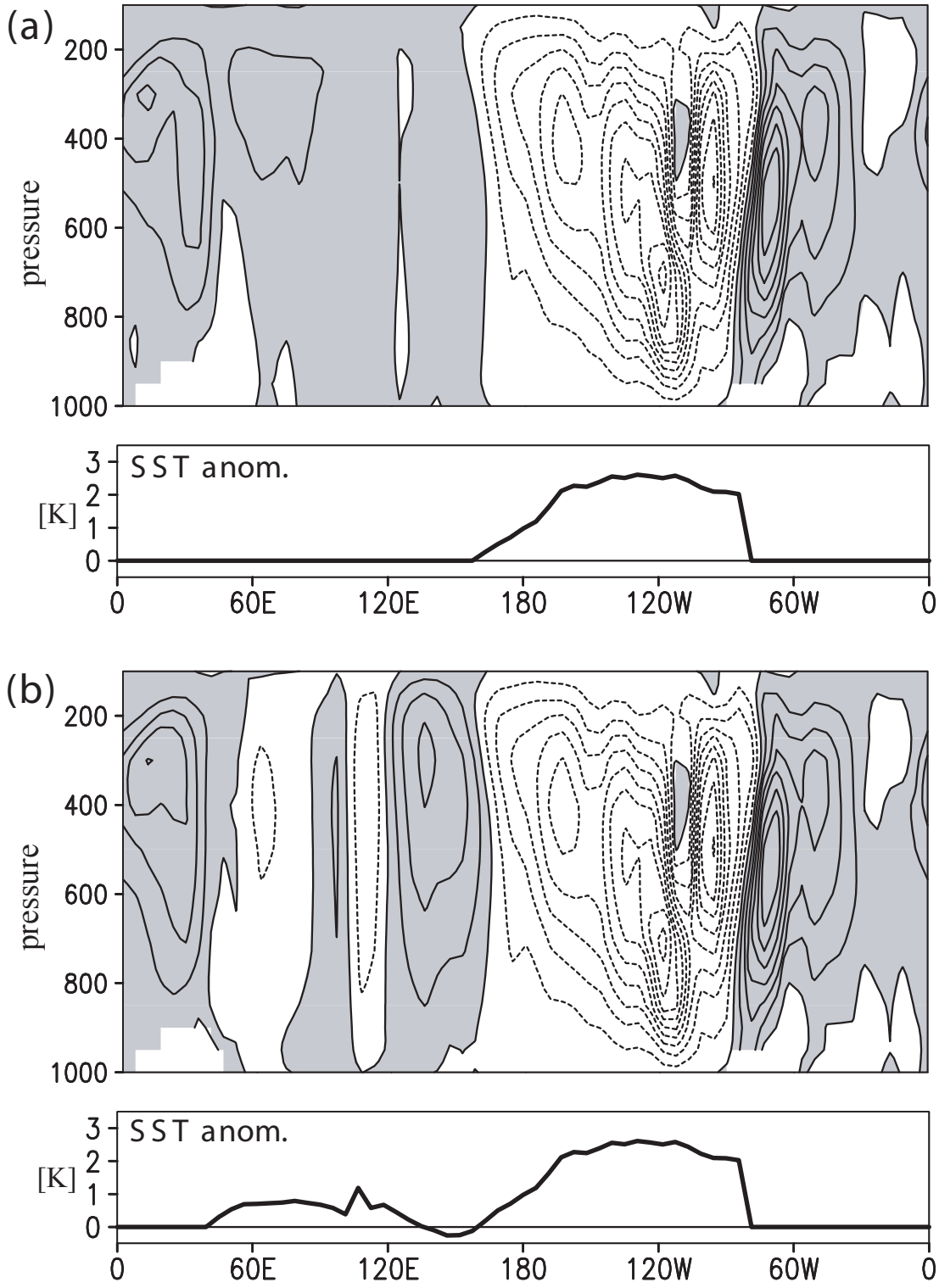
(a)
200
400
600
800
1000
pressure
SST anom.
[K]
3
2
1
0
0
60E
120E
180
120W
60W
0
(b)
200
400
600
800
1000
pressure
SST anom.
[K]
3
2
1
0
0
60E
120E
180
120W
60W
0

Figure 11.

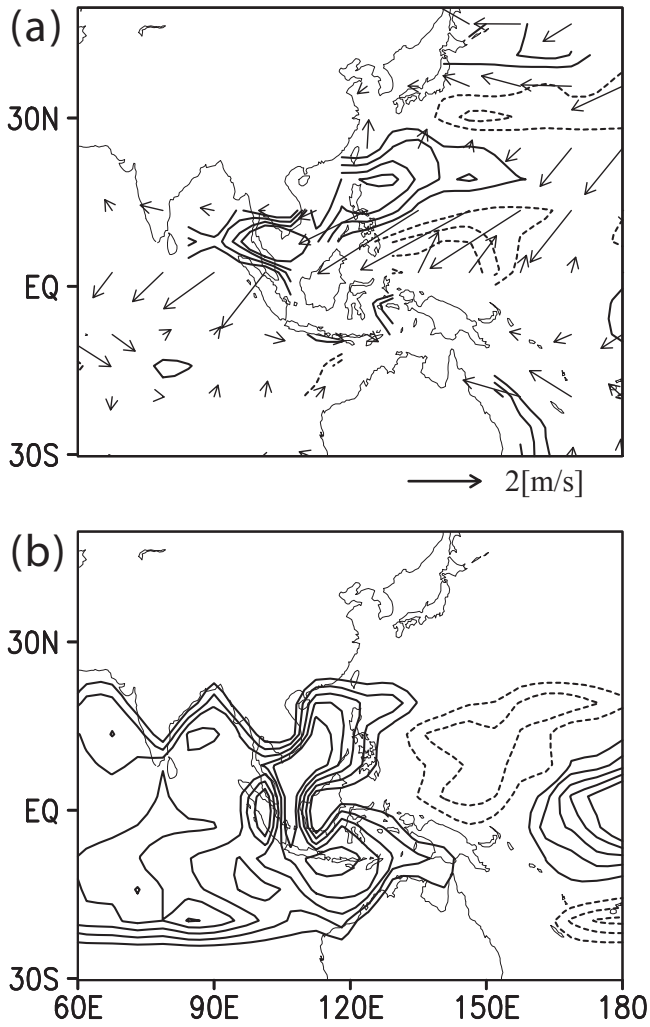


Figure 12.

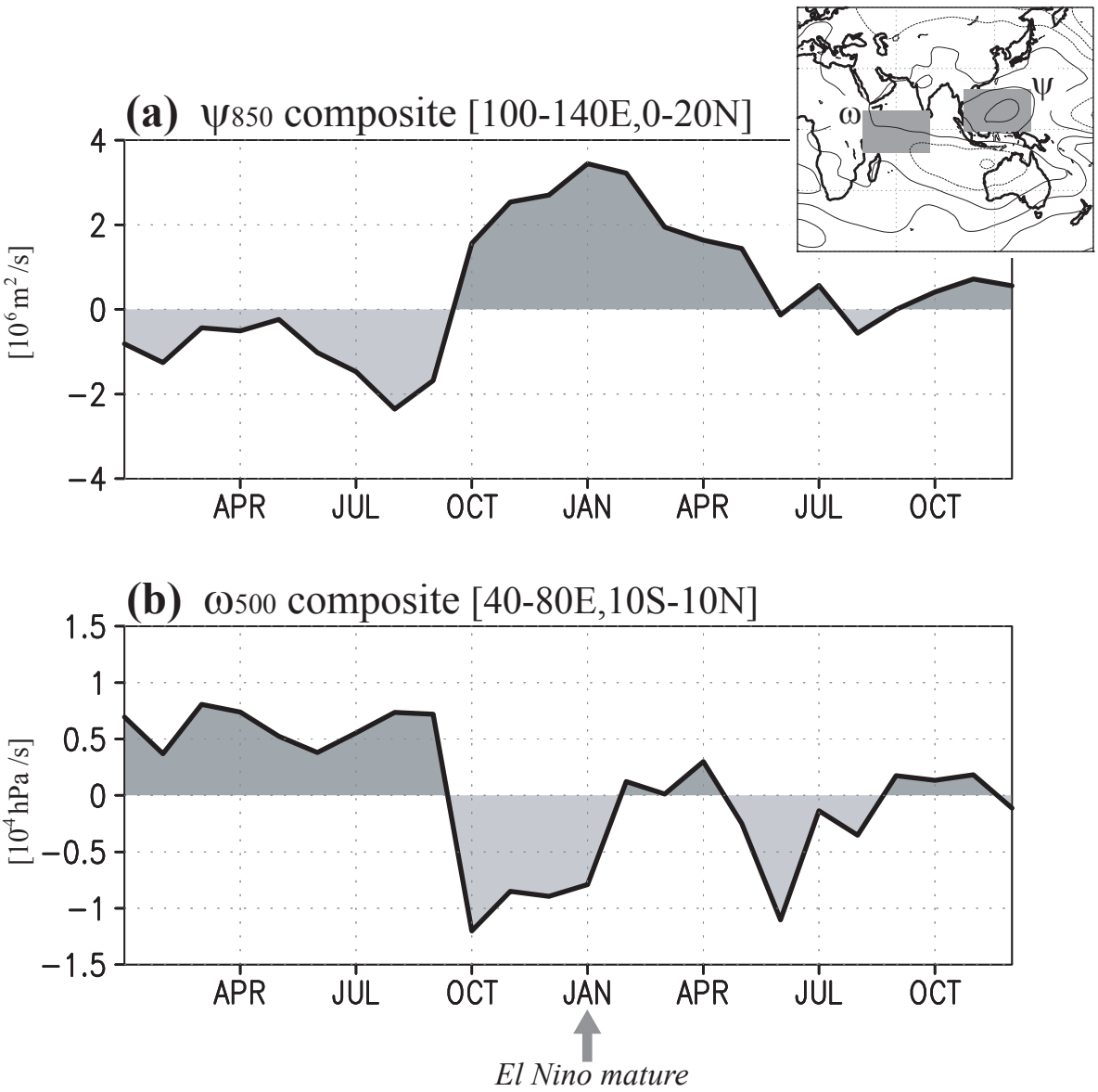
(a) ψ850 composite [100-140E,0-20N]
ψ
ω
[10^6 m^2 /s]
4
2
0
−2
−4
APR
JUL
OCT
JAN
APR
JUL
OCT
(b) ω500 composite [40-80E,10S-10N]
[10^4 hPa /s]
1.5
1
0.5
0
−0.5
−1
−1.5
APR
JUL
OCT
JAN
APR
JUL
OCT
El Nino mature

Figure 13.

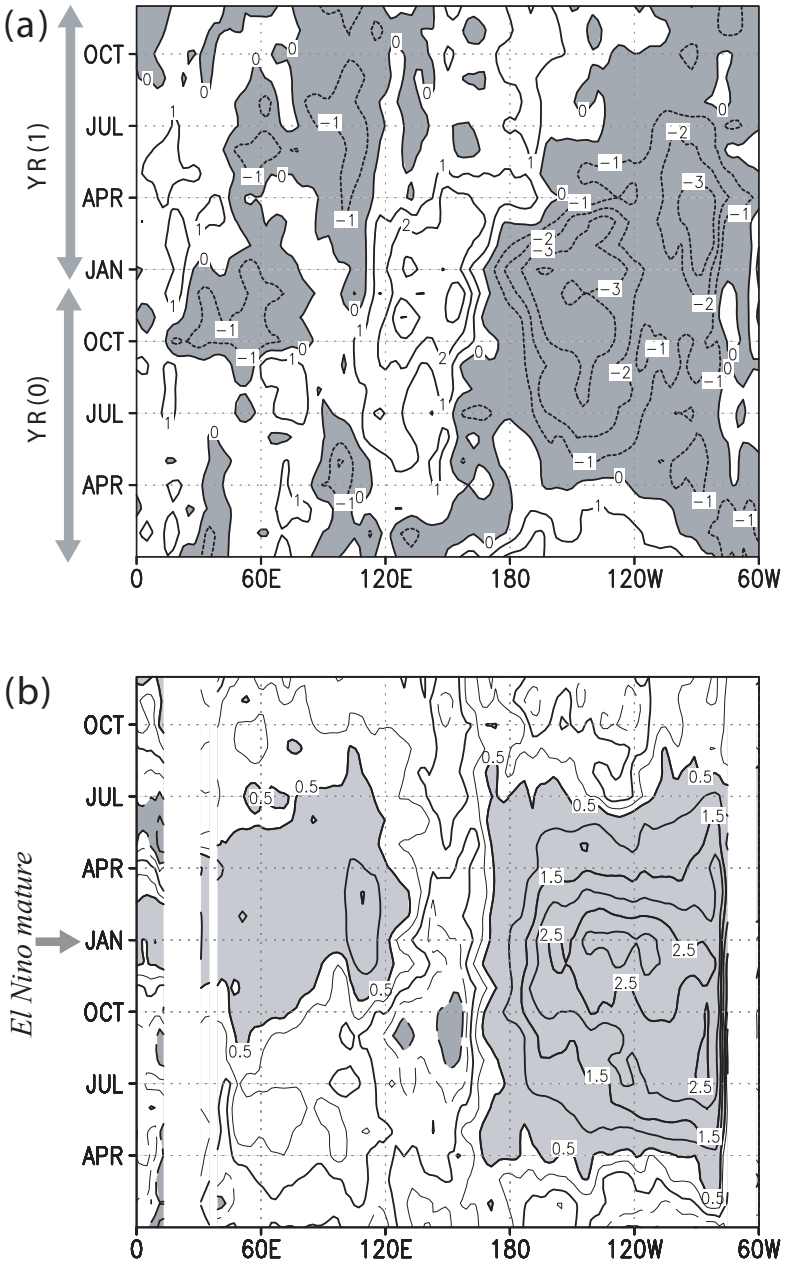
(a)
YR(1)
YR(0)
OCT
JUL
APR
JAN
OCT
JUL
APR
0
60E
120E
180
120W
60W
(b)
El Nino mature
OCT
JUL
APR
JAN
OCT
JUL
APR
0
60E
120E
180
120W
60W

Figure 14.

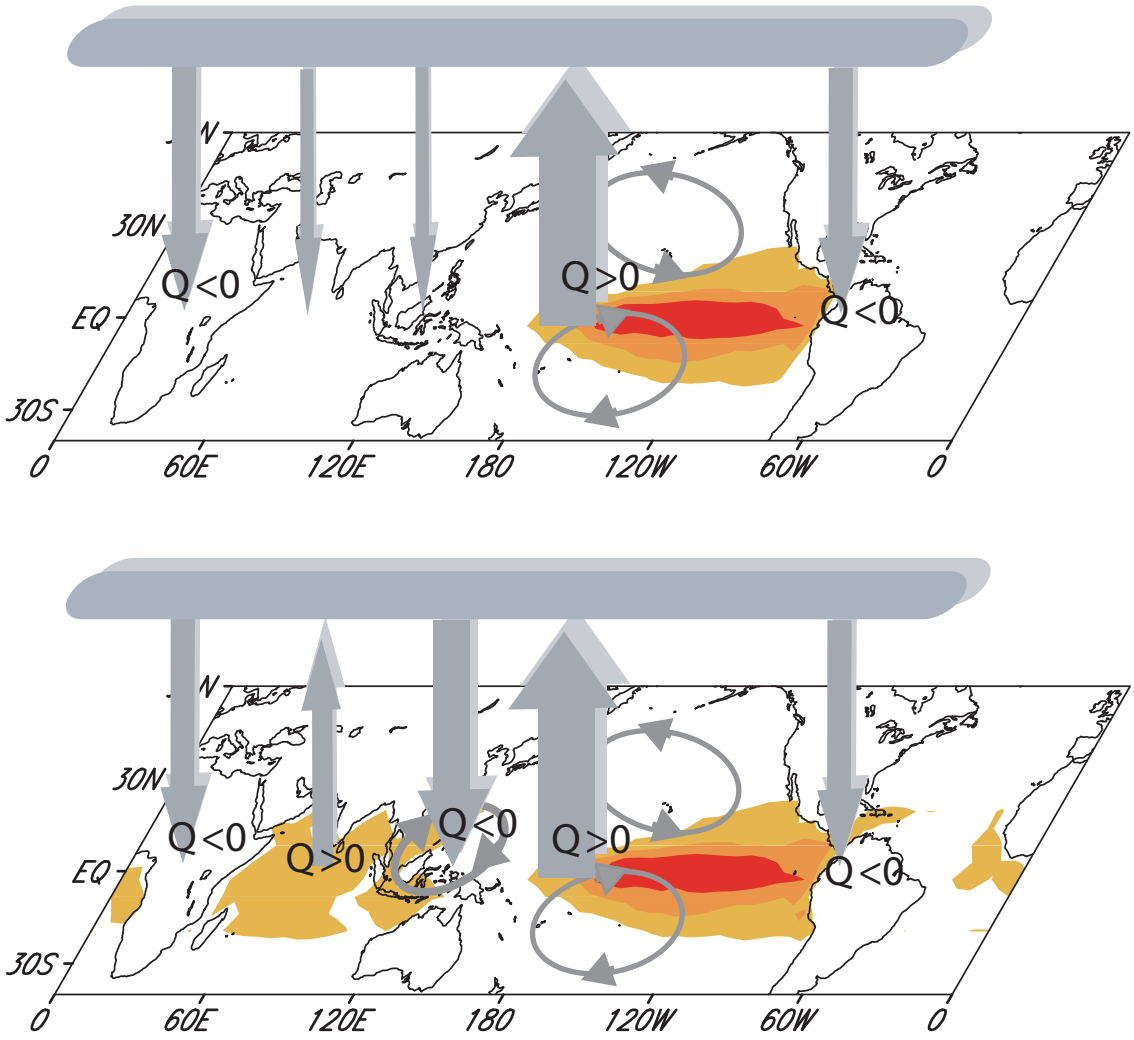
N
30N
EQ
30S
0
60E
120E
180
120W
60W
0
Q<0
Q>0
Q<0
N
30N
EQ
30S
0
60E
120E
180
120W
60W
0
Q<0
Q>0
Q<0
Q>0
Q<0

Figure 15.

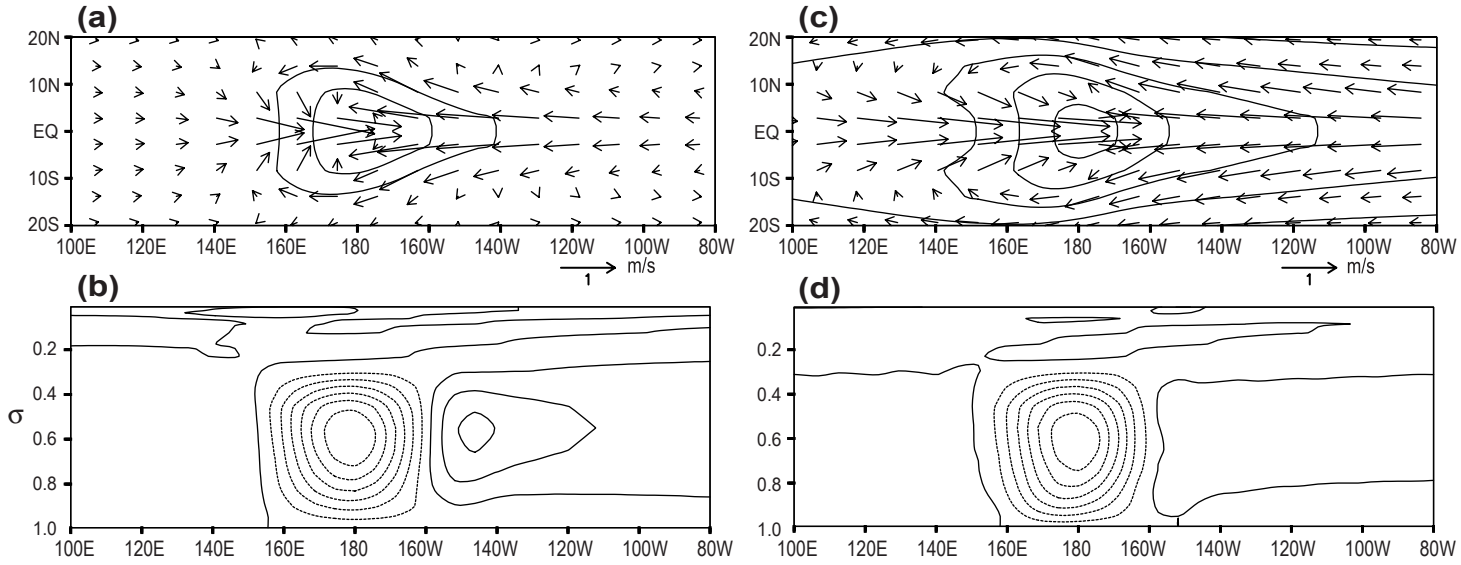
(a)
(b)
(c)
(d)
20N
10N
EQ
10S
20S
100E
120E
140E
160E
180
160W
140W
120W
100W
80W
1
m/s
σ
0.2
0.4
0.6
0.8
1.0

Figure A1.

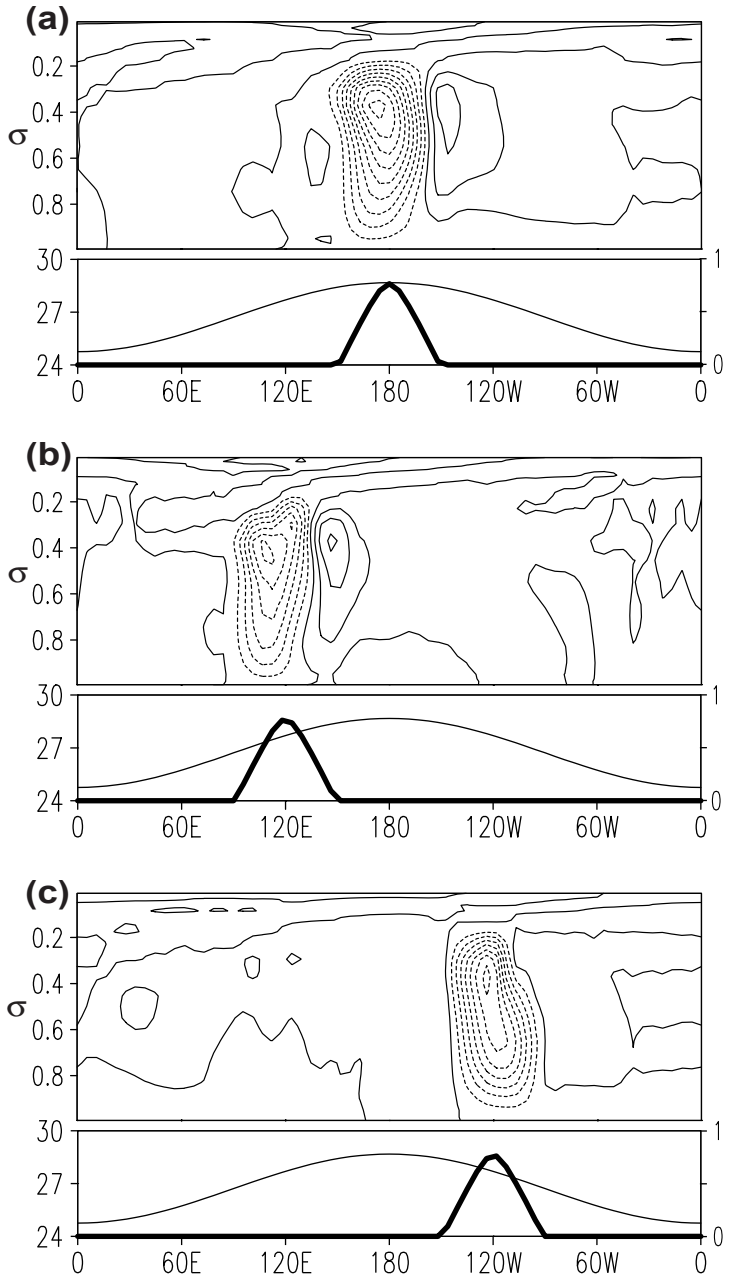


Figure A2.